Table of Contents

12. Supplementary Figures

1. Introduction

In this Supplementary Information we provide further information regarding the study design, materials and methods, and additional data. The materials and methods section provide detailed description of the collection, dissection methods, and quality control assessments of postmortem human brain tissue used in this study. We provide technical descriptions of data generation and analyses using different platforms. We also make available additional data that were discussed in the main manuscript. Finally, we present supplementary figures and tables generated from sample metadata and specific gene lists.

2. Supplementary Information on the Study Design

2.1. Definition of periods of human development and adulthood used in this study

Brain development is a highly dynamic process during which different regions undergo distinct maturational changes. Moreover, transient brain structures arise and disappear during specific developmental periods. Thus it was crucial that multiple regions and major developmental time points were analyzed to allow for the identification of temporally and spatially specific transcriptional changes. We created a classification system of human brain development and adulthood comprised of 15 periods emphasizing the timing and progression of major neurodevelopmental events in the cerebral cortex, a structure that is central to the highest cognitive functions in humans and is arguably one of the most studied human brain structures. Our aim in classifying specimens into different periods was to broadly compare our data to the majority of published data and to have the precision to allow for detection of transcriptional changes that may occur with high temporal specificity during prenatal and early postnatal periods.

At the present, well-defined morphological staging is limited to the embryonic development (the well-known Carnegie stages[51]), and no fully satisfactory staging system has yet been devised for the fetal and early postnatal development. To avoid confusion with the Carnegie stages, we divided our specimens into periods covering both development and adulthood, taking into consideration previous developmental classifications of the human brain[51-56]. Although prenatal development is relatively short in comparison to postnatal development, it is highly dynamic. We divided prenatal development into seven distinct periods to facilitate higher temporal resolution. For postnatal developmental periods, we considered cognitive, motor, social, and emotional milestones outlined by the Department of Human Health and Services (http://www.cdc.gov/ncbddd/child/). As previously elaborated[51], prenatal age is with respect to fertilization by definition. For prenatal age we used postconceptional weeks (PCW) to include both proper terms used in current literature: postfertilizational (timed from the fertilization of the ovum) and postovulatory (timed from the ovulation). Although there is a small difference in the timing of these events, for the majority of purposes these three terms (postconceptional, postfertilizational and postovulatory) could be used synonymously. The following is a brief description of the periods as defined in this study.

___Period 1___ (Embryonic development, $4 \leq$ Age < 8 PCW) corresponds to late embryonic development defined by the first lamination of the cerebral wall (i.e., ventricular zone, intermediate zone, marginal zone). Early embryonic processes (e.g., formation of the neural tube, closure of the neuropores, and formation of the primary and secondary brain vesicles) are completed in this period. This period is marked by extensive proliferation and the initiation of neurogenesis. The first axons invade the cerebral wall during this period.

Period 2 (Early fetal development, 8≤ Age <10 PCW) is characterized by the appearance and subsequent primary consolidation of the cortical plate. Deep layer neurons are generated and begin to radially migrate to their proper position in the cortical plate. The secondary proliferative zone, the subventricular zone, appears around 8 PCW. The internal capsule and anterior commissure begin to appear. Major neuroanatomical fetal landmarks are readily recognized during this period, including the ventricular zone, subventricular zone, intermediate zone, presubplate zone (i.e., precursor of future subplate proper), cortical plate, marginal zone, and subpial granular layer can be distinguished in the cerebral wall.

Period 3 (Early fetal development, 10≤ Age <13 PCW) is characterized by the presence of the bilaminate cortical plate. Namely, the deep part of the cortical plate itself becomes delaminated and together with a thin, cell-sparse band of tissue (described as the presubplate in the previous period) represents the subplate in formation. The first synapses are formed in the marginal zone above the cortical plate and in the presubplate zone below the cortical plate, whereas the cortical plate remains free of synapses. Tangential migration of GABAergic interneurons can be observed. Proliferation and migration of neurons are the two main histogenetic processes that occur during this period. The corpus callosum can be identified during this period. Afferent projections start to invade the cortical anlage and are primarily monoaminergic. The first sulci start to appear in this period (i.e., lateral and callosal sulcus).

Period 4 (Early mid-fetal development, 13≤ Age <16 PCW) is characterized by the secondary consolidation of the cortical plate concomitantly with the formation of a large, synapse-rich subplate zone. The first cortical neurons show signs of morphological differentiation. After its formation and during subsequent mid-fetal periods, the subplate zone serves as a waiting compartment for afferent axons from several subcortical structures. Proliferation and migration of neurons and ingrowth of afferent axons are the major histogenetic events occurring during this period. At this period and subsequent prenatal periods, typical fetal lamination pattern of the cerebral wall can be observed. The cerebral wall can be divided into six major architectonic compartments or fetal zones: ventricular zone, subventricular zone, intermediate zone, subplate zone, cortical plate, and marginal zone, which contains a transient subpial granular layer.

Period 5 (Early mid-fetal development, 16≤ Age <19 PCW) is characterized by an increase in the size of the subplate zone and the overall thickness of the cerebral wall. Ingrowth of thalamocortical axons into the subplate and migration of upper cortical layer projection neurons are major histogenetic events. The parieto-occipital, cingulate, and calcarine sulci appear in this period.

Period 6 (Late mid-fetal development, 19≤ Age <24 PCW) is characterized by the peak of subplate zone thickness and development, and by the massive ingrowth of afferent axons from the subplate zone into the cortical plate. Therefore, the first synapses can be observed in the neocortical plate. Neurogenesis ceases in the pallial wall but still continues in the subpallial ganglionic eminences during this period. The central sulcus, superior temporal sulcus, collateral sulcus, superior temporal gyrus, and parahippocampal gyrus can be identified.

Period 7 (Late fetal development, 24≤ Age <38 PCW) is characterized by the transformation of the typical fetal lamination pattern into an adult-like lamination pattern of the cerebral wall. Resolution of the subplate zone starts and the Brodmann's "six-layered ontogenetic Grundtypus" (i.e., the fetal equivalent of future layers 2–6) appears within the cortical plate during this period. Cytoarchitectonic regional and areal differentiation of the cortical plate/cortex is an important event that occurs during this period. Neuronal differentiation, ingrowth of thalamocortical axons, and gliogenesis are major histogenetic processes observed

during this period. Synaptogenesis continues primarily in the cortex. Myelination of select cortical axon projections starts in this period. The ventricular zone gradually thins until it appears as a single layer of cuboidal/columnar cells. Majority of cortical gyri and sulci appear during this period.

Period 8 (Neonatal and early infancy, birth ≤ Age <6 postnatal months) is characterized by reorganization of long afferent and corticocortical axons, transformation and maturation of cortical layers (especially layer 5 and 6) from a fetal to an adult-like pattern, and rapid synaptogenesis and spinogenesis. The remnants of the subplate zone, although resolving, are still present below layer 6 and thus form a transition from immature cortex to the developing gyral white matter. Specific motor (e.g., grasping, raising of the head, stretching of the legs and kicking) and sensory (e.g., object following, head turning toward sound) skills appear during this period.

Period 9 (Late infancy, 6≤ Age <12 postnatal months) is characterized by further development of motor skills (e.g., sitting with and without support), sensory skills (e.g., development of color vision), and cognitive skills (e.g., exploration with hand and mouth, response to one's own name). Resolution of the subplate zone is completed and neurons that survive resolution of the subplate zone are incorporated into the subcortical (gyral) white matter as interstitial neurons.

Period 10 (Early childhood, 1≤ Age <6 years) is characterized mainly by reorganization and maturation of local circuits, and the peak of synaptogenesis. During this period rapid development of motor skills (e.g., walking, pincer grasp, fine movement control), social and emotional skills (e.g., development of imitation, self-awareness, independence), and cognitive skills (e.g., thinking, mathematical abilities, language) is observed.

Period 11 (Middle and late childhood, 6≤ Age <12 years) is characterized by further cognitive development and refinement of neural circuits.

Period 12 (Adolescence, 12≤ Age <20 years) is characterized by sexual maturation and the appearance of adult-like connectivity pattern.

Period 13 (Young adulthood, 20≤ Age <40 years) is characterized by the end of maturation processes in the brain (e.g., myelination ends in the first part of this period) and the appearance of an adult-pattern of brain functions.

Period 14 (Middle adulthood, 40≤ Age <60 years) is characterized by an adult-like pattern of brain functions and the beginning of aging processes.

Period 15 (Late adulthood, 60 years +) is characterized by the progression of aging processes.

2.2. Ontology and anatomical definition of sampled brain regions and NCX areas
Brain development is a highly dynamic process during which each region undergoes distinct organizational and maturational changes. Thus we created a structural ontology that contains brain structures (e.g., NCX areas, HIP, AMY, STR, MD, CBC) that are well defined throughout most of time periods and several transient structures (e.g., MGE, LGE, CGE, URL). In total, 8 structures were analyzed for period 1, 10 regions for period 2 and up to 16 regions for periods 3–15. Below we describe this ontology and anatomical definition of sampled brain regions and NCX areas based on histological verification.

2.2.1. Neocortex (NCX)

Samples collected from period 1 and 2 specimens contained the entire thickness of the cerebral wall. Samples collected from period 3–7 specimens contained the marginal zone, cortical plate, and part of the underlying subplate (Supplementary Fig. 3). Samples from period 8–15 specimens were dissected such that the entire gray matter (layer 1-6) and part of the underlying subplate (periods 8 and 9) or white matter (periods 10 – 15) were collected (Supplementary Fig. 3). Nissl staining of the neighbouring thin block was used to histologically verify the identity of the dissected area and to microscopically evaluate tissue. Neocortical cytoarchitecture of each sample was compared to areal cytoarchitectonic maps to distinguish Brodmann areas (BA)[57]. Samples with incorrect cytoarchitecture or abnormal microscopical appearance were excluded from the study. Neocortical areas (see below) were grouped according to the lobes from which they were sampled.

2.2.1.1. Frontal cortex (FC)

For *period 1*, the sampled area corresponded to the anterior third of telencephalic vesicle (cerebral wall) corresponding to prospective FC.

For *period 2*, the sampled area corresponded to different parts corresponding to prospective FC: orbital (OFC), dorsolateral (DFC), ventrolateral (VFC), and medial (MFC) of the anterior part of telencephalic vesicle (cerebral wall). In addition, paracentral region corresponding approximately to the prospective motor and parietal somatosensory (M1C/S1C) cerebral wall was dissected as one sample (MSC).

For *periods 3–7*, prior to the appearance of all gyri and sulci, multiple areas of the FC were sampled as follows (Supplementary Fig. 2):

- **Orbital prefrontal cortex (OFC)** was sampled from the middle part of the orbital surface of the cerebral hemisphere, immediately next to the prospective gyrus rectus.
- **Dorsolateral prefrontal cortex (DFC)** was sampled from the middle third of the dorsolateral surface of the anterior third of the cerebral hemisphere.
- **Ventrolateral prefrontal cortex (VFC)** was sampled from the posterior part of the frontal operculum, above the lateral sulcus and prospective insula.
- **Medial prefrontal cortex (MFC)** was sampled from the perigenual and subgenual region of the medial surface.
- **Primary motor cortex (M1C)**, prior to the appearance of the central sulcus, was sampled from the anterior third of the middle third of the cerebral hemisphere, medial third and upper part of the lower third of the dorsolateral surface. We used the striatum at the septal level as the landmark between the anterior and middle one third of the dorsolateral cortical surface. In some cases, we sampled M1C and S1C areas as single area and termed it motor-somatosensory cortex (**M1C/S1C**) due to the lack of clear anatomical and histological boundaries between immature M1C and S1C. After the appearance of the central sulcus M1C was sampled in front of the central sulcus from the middle and upper part of the lower third of the dorsolateral surface of the hemisphere.

For *periods 8–15*, sampled areas were as follows (Supplementary Fig. 1):

- OFC was sampled from the anterolateral two thirds of the orbital gyri. OFC corresponds approximately to BA 11.
- DFC was sampled from approximate border between the anterior and middle third of the medial frontal gyrus. DFC corresponds approximately to BA 9 and 46.

- VFC was sampled from the posterior third of the inferior frontal gyrus, corresponding to the opercular and triangular part of the inferior frontal gyrus. VFC corresponds approximately to BA 44 and 45.
- MFC was sampled from perigenual and subgenual parts of the anterior cingulate gyrus and the anteromedial part of the superior frontal gyrus. MFC corresponds approximately to BA 24, 32 and 33.
- M1C was sampled from the ventrolateral part of the precentral gyrus, corresponding most closely to the orofacial region of M1C. M1C corresponds to BA4.

2.2.1.2. Parietal cortex (PC)

For *period 1*, the sampled areas corresponded to the dorsal middle third of the cerebral wall.

For *period 2*, the sampled areas included the paracentral region corresponding approximately to the prospective motor and parietal somatosensory (M1C/S1C) cerebral wall, and the posterior half of the dorsal middle third of the cerebral wall corresponding approximately to the prospective inferior parietal cortex (IPC).

For *periods 3–7*, prior to the appearance of gyri and sulci, multiple areas of the PC were sampled as follows (Supplementary Fig. 2):

- **Primary somatosensory cortex (S1C)**, prior to the appearance of the central sulcus, was sampled immediately caudal to the M1C (see M1C description above). After the appearance of the central sulcus, S1C was sampled behind the central sulcus from the middle and upper part of the lower third of the dorsolateral surface of the cerebral hemisphere adjacent to the M1C area.
- **Posterior inferior parietal cortex (IPC)** was sampled from the lower posterior part of the dorsolateral surface of the middle third of the cerebral hemisphere adjacent to the end of the lateral sulcus.

For *periods 8–15*, sampled areas were as follows (Supplementary Fig. 1):

- S1C was sampled from the ventrolateral part of the postcentral gyrus adjacent to the M1C area. S1C corresponds to BA 1–3.
- IPC was sampled from the posterior half of the supramarginal gyrus. IPC corresponds approximately to BA 40.

2.2.1.3. Temporal cortex (TC)

For *period 1*, the sampled area corresponded to the anterior two thirds of the lateral part of the posterior third of the cerebral wall.

For *period 2*, the sampled areas included the posterior two thirds of TC corresponding approximately to the prospective auditory and superior temporal cortex (A1C/STC) cerebral wall, and the anterior third corresponding approximately to the prospective inferior temporal cortex (ITC).

For *periods 3–7*, prior to the appearance of gyri and sulci, multiple areas of the TC were sampled as follows (Supplementary Fig. 2):

- **Primary auditory cortex (A1C)** was sampled from the upper part of the temporal bank of the lateral sulcus.
- **Posterior superior temporal cortex (STC)** was sampled from the upper part of the superior third of the temporal lobe adjacent to the lateral sulcus and A1C area.

- **Inferior temporal cortex (ITC)** was sampled from the lower part of the inferior third of the temporal lobe adjacent to the temporal lobe pole.

For *periods 8–15*, sampled areas were as follows (Supplementary Fig. 1):
- A1C was sampled from the planum temporale and the transverse temporal gyri. A1C corresponds to BA 41.
- STC was sampled from the posterior third of the superior temporal gyrus. STC corresponds approximately to BA 22.
- ITC was sampled from the anterior third of the inferior temporal gyrus. ITC corresponds approximately to BA 20.

2.2.1.4. Occipital cortex (OC)

For *periods 1 and 2*, sampled tissue corresponded to the posterior (occipital) part of the cerebral wall.
For *periods 3–7*, (Supplementary Fig. 2) prior to the appearance of gyri and sulci, sampled tissue corresponded to prospective **primary visual cortex** (**V1C**). Prior to the appearance of the calcarine fissure, V1C was sampled from the posterior third of the medial wall of the prospective occipital lobe. After appearance of the calcarine fissure, V1C was sampled as described below.

For *periods 8–15*, (Supplementary Fig. 1) V1C was sampled from the area surrounding the calcarine fissure. Only samples in which the stria of Gennari could be recognized were included. V1C corresponds to BA 17. Small pieces of the neighbouring BA18 could have been occasionally present in the sample, but the majority of the sample corresponded to BA17.

2.2.2. Hippocampus (HIP)

For *periods 1 and 2*, HIP was sampled from the hippocampal anlage, located on the ventromedial side of the cerebral hemisphere.

For *periods 3–15*, (Supplementary Figs 1 and 2) HIP was sampled from the middle third of the retrocommissural hippocampal formation, located on the medial side of the temporal lobe. Sampled areas always contained dentate gyrus and the cornu ammonis. Samples dissected from the frozen tissue may contain small quantities of the neighbouring choroid plexus.

2.2.3. Amygdala (AMY)

We aimed at dissecting the whole AMY from *period 3–15* specimens (Supplementary Figs 1 and 2). Very small quantities of surrounding white matter and potentially other surrounding structures in the basal telencephalon were included in samples.

2.2.4. Ventral forebrain (VF)

Depending on the time period we sampled different parts of the VF. For *period 1*, the sampled region corresponded to the ventral forebrain (VF), which included primordium of the ganglionic eminence.

2.2.4.1. Medial ganglionic eminence (MGE)
2.2.4.2. Lateral ganglionic eminence (LGE)
2.2.4.3. Caudal ganglionic eminence (CGE)

We sampled the MGE, LGE and CGE separately from *period 2* specimens. Small quantities of surrounding tissue may be included in the samples.

2.2.4.4. Striatum (STR)

Striatum (**STR**) was sampled from *periods 3–15* specimens (Supplementary Figs 1 and 2). We dissected the anterior part of striatum containing the head of the caudate nucleus and the putamen, separated by the internal capsule and ventrally connected to the nucleus accumbens. Small quantities of surrounding white matter are included in the samples.

2.2.5. Diencephalon (DIE)

Depending on the time period, we sampled different parts of the DIE. For *period 1*, the sampled region corresponded to the entire DIE.

2.2.5.1. Dorsal thalamus (DTH)

For *period 2*, the sampled region corresponds to the dorsal part of the thalamic anlage (**DTH**).

2.2.5.2. Mediodorsal nucleus of the thalamus (MD)

For *periods 3–15* (Supplementary Figs 1 and 2), the whole mediodorsal nucleus of the thalamus (**MD**) was sampled from the dorsal and medial thalamus. Small quantities of surrounding thalamic nuclei could be present in the samples.

2.2.6. Upper (rostral) rhombic lip (URL)

Sampled region corresponds to the **URL** and adjacent tissue located above the upper rhomboid fossa for *periods 1 and 2*.

2.2.6.1. Cerebellar cortex (CBC)

CBC was sampled from the lateral part of the posterior lobe for *periods 3–15* (Supplementary Figs 1 and 2). The sampled area contained all three layers of cerebellar cortex and underlying white matter but not the deep cerebellar nuclei. CBC approximately corresponds to the lateral pontocerebellum.

2.3. Workflow of quality control measures

To summarize the quality control (QC) measures taken in this study, we have made a diagram (Supplementary Fig. 5) showing QC steps during the generation of the dataset. Five QC steps were performed on 94 brains that were considered for this study. The first QC step was assessment of donors and tissue (see exclusion criteria in Supplementary section 3.3). Twenty-three brains did not pass the first QC step and were excluded from further analysis. Of the remaining 71 brains that were included, 58 of them were subsequently processed (as of December 2010) and remaining brains are currently being processed. The second QC step was assessment of dissection process based on dissection score (DS; for explanation see Supplementary section 3.4.3). There were 74 dissected samples that did not pass this QC step, leaving 1,414 samples from 58 brains that were processed and from which RNA extracted for further analysis. The third QC step was control of RNA quality based on RNA integrity number (RIN; see Supplementary section 5.1), and 15 samples did not pass as they did not fulfill our cutoff set at RIN ≤5. The fourth QC step was assessment of preparation and hybridization of RNA samples to the Affymetrix microarray chip (see Supplementary section 5.3). Following the removal of 53 samples after this QC step, 1,346 samples were successfully processed on Affymetrix microarray chips and analyzed for gene expression. The fifth QC step was detection of outliers. There were five samples, all from a single brain, excluded on this basis of hierarchical sample clustering (see Supplementary section 5.4, paragraph 1). One additional sample was excluded by correlation analysis (see

Supplementary section 5.4, paragraph 2). As of December 2010, 1,340 microarray samples passed QC steps and were included in this study.

3. Tissue Procurement and Sampling

3.1. Tissue procurement

This study was conducted using postmortem human brain specimens from tissue collections at the Department of Neurobiology at Yale University School of Medicine and the Clinical Brain Disorders Branch of the National Institute of Mental Health. Additional specimens were procured from the Human Fetal Tissue Repository at the Albert Einstein College of Medicine (AECOM), the Brain and Tissue Bank for Developmental Disorders at the University of Maryland, the Birth Defects Research Laboratory at the University of Washington, Advanced Bioscience Resources Inc. and the MRC-Wellcome Trust Human Developmental Biology Resource at the Institute of Human Genetics, University of Newcastle, UK. Tissue was collected after obtaining parental or next of kin consent and with approval by the institutional review boards at the Yale University School of Medicine, the National Institutes of Health, and at each institution from which tissue specimens were obtained. Tissue was handled in accordance with ethical guidelines and regulations for the research use of human brain tissue set forth by the NIH (http://bioethics.od.nih.gov/humantissue.html) and the WMA Declaration of Helsinki (http://www.wma.net/en/30publications/10policies/b3/index.html).

Appropriate informed consent was obtained and all available non-identifying information was recorded for each specimen. Specimens range in age from 5.7 weeks postconception (PCW) to 82 years. Of 57 postmortem brain specimens included in this study, 18 were obtained with either left or right hemisphere, and 39 were obtained with both hemispheres. Embryonic and fetal age was extrapolated based on the date of the mother's last menstruation, characteristics of the fetus noted upon ultrasonography scanning, foot length of the fetus, and visual inspection. The postmortem interval (PMI) was defined as hours between time of death and time when tissue samples were frozen.

3.2. Neuropathological evaluation

All clinical histories, tissue specimens, and histological sections were evaluated to assess for hypoxia, cerebrovascular incidents, tumours, microbial infections, neurodegeneration, demyelination, and metabolic disease. In addition, cadavers from period 4 onward underwent a complete autopsy and were refrigerated beforehand to minimize degradation. To prepare tissue sections for microscopic neuropathological examination, small samples (usually the dorsal parietal cortex, striatum with ependymal layer and subependymal zone, hippocampus, and the cerebellar cortex) of fresh or frozen tissue were dissected and fixed in 4% paraformaldehyde and processed for histology and immunohistochemistry as described below.

3.3. Selection criteria for brain specimens

To better ensure consistency between samples and decrease potential variation due to ante- and postmortem conditions, specific selection criteria were arbitrarily established. Most postnatal and adult brains also underwent comprehensive toxicological screening. The aim was to collect tissue specimens from clinically unremarkable donors without history or signs of neurological or neuropsychiatric illness or drug abuse. The following selection criteria were strictly adhered to when deciding whether to exclude or include each brain specimen.

- Brains with chromosomal or large-scale genomic abnormalities, detected by karyogram and/or Illumina Human Omni-2.5, were excluded.

- Prenatal and neonatal specimens were excluded if drug or alcohol abuse by the mother during pregnancy was reported or if potassium chloride, salt water, or urea were injected into the amniotic sac during surgical procedure.
- Only brains free of obvious malformations or lesions were collected. Disqualifying characteristics included any obvious abnormality of the neural tube, forebrain, brainstem, cranial nerves, cerebellum, or spinal cord (i.e., prominent intraparenchymal haemorrhage and ischemia, infection, periventricular leukomalacia, abnormal meninges, dysplasia, hypoplasia, alterations in the pial or ventricular surface, and extensive white matter lesions).
- Samples were excluded if microscopic analysis revealed extensive neuronal loss, neuronal swelling, glioneuronal heterotopias, or dysmorphic neurons and neurites.
- Samples that tested positive for Hepatitis B, Hepatitis C, or HIV were excluded.
- Early postnatal and adult (periods 8–15) specimens were excluded if excessive drug or alcohol abuse was reported, if the individual had any known neurological or psychiatric disorders, or if any prolonged agonal conditions (coma, prolonged pyrexia, hypoxia, seizures, prolonged dehydration, hypoglycaemia, and multiple organ failure) were reported. Other excluding factors included ingestion of neurotoxic substances at the time of death, suicide, severe head injury, significant haemorrhages, widespread vascular abnormalities, ischemia, tumours, stroke, congenital neural abnormalities, and signs of neurodegeneration (spongiosis, amyloid plaques, neurofibrillary tangles, Lewy bodies, and amyloid angiopathy).

3.4. Tissue processing and dissections

Depending on the condition and period of the procured specimens, four different dissection methods were used. Photos and/or video were used to document dissections using digital cameras. Regions of interest were matched between different specimens, ages, and hemispheres of each brain. Supplementary Table 3 provides a complete list of all tissue samples included in this study. Specific dissection protocol depended upon the period of the specimen and the method by which it was preserved. For all brain specimens procured at Yale University School of Medicine and the Human Fetal Tissue Repository at AECOM, brain regions and NCX areas of interest were collected from fresh tissue. For all other specimens, regions/areas were collected from frozen tissue slabs or whole specimens stored at -80 ºC. To ensure consistency between specimens, all dissections were performed by the same person. Small samples of fresh or frozen URL (period 1 and 2) or CBC (period 3-15) were used to measure tissue pH.

3.4.1. Tissue dissection methods

Different dissection procedures were used for each specimen, depending upon the period of the brain (see below). Our pilot experiments indicated that the quality of RNA and DNA was largely unaffected by variation between the dissection methods used.

3.4.1.1. Regional sampling from fresh brain specimens

Brains were chilled on ice for 15–30 minutes prior to sectioning. Brains were placed ventral side up onto a chilled aluminium plate (1 cm thick) on ice. The brainstem and cerebellum were removed from the cerebrum by making a transverse cut at the junction between the diencephalon and midbrain. Next, the cerebrum was divided into left and right hemispheres by cutting along the midline using a Tissue-Tek Accu-Edge trimming blade, 260 mm. The cerebellum was separated from the brainstem by cutting directly posterior to the brainstem, along the cerebellar peduncles. The regions of interest were dissected using a scalpel blade and immediately frozen in liquid nitrogen. Dissected samples were either immediately processed for RNA extraction or stored at -80 °C for later RNA extraction. The remaining brain tissue was

cut to obtain 1 cm (period 5–15 specimens) or 0.5 cm (periods 3 and 4 specimens) thick serial, coronal sections. The tissue slabs were snap frozen in isopentane (J.T. Baker)/dry ice at -30 to -40 ºC and stored at -80 ºC.

3.4.1.2. Regional sampling from frozen brain specimens
All previously frozen periods 3–15 specimens and tissue slabs were microscopically inspected and the desired region was demarcated, then dissected using a dental drill (AnyXing, 300D) and a Lindemann Bone Cutter H162A.11.016 or diamond disk saw (Dental Burs USA; r=11 mm) on a 1 cm thick aluminium plate over dry ice. Dissected tissue samples were stored at -80 ºC prior to further processing.

3.4.1.3. Regional sampling from specimens processed in RNA*later* ICE
Frozen period 1 and 2 specimens were sectioned coronally at approximately 2 mm, beginning at the frontal pole, using a dental diamond disk saw. For gradual thawing, tissue slabs were transferred from -80 °C storage to overnight storage in RNA*later* ICE (Ambion) at -20 °C. Tissue slabs were visually inspected for gross anatomical neuropathological abnormalities. Next, regions of interest were sampled under a dissection microscope at 4 °C and stored in Buffer RLT Plus from the RNeasy Plus Mini Kit (Qiagen) at 4 °C. RNA was immediately extracted.

3.4.2. Histological verification of tissue sampling
To verify that the region or NCX area of interest is properly and consistently sampled, we also collected small tissue blocks, from both frozen and fresh brain specimens, adjacent to the tissue sample dissected for the RNA extraction. We have done this for the majority of M1C, S1C, IPC, A1C and V1C samples, which in our experience were hard to match across different specimens but can be histologically verified using Nissl method in postnatal specimens due to cytoarchitectonic differences. This method was also occasionally used for other regions or NCX areas. These tissue blocks were then fixed in 4% paraformaldehyde for 48 h, sectioned at 50 µm thickness using a vibratome, and Nissl stained to verify the identities of dissected adjacent tissue (examples of Nissl stained brain regions and NCX areas from a fetal and adult brain are provided in Supplementary Fig. 3).

3.4.3. Dissection scoring
We developed a scoring system to evaluate the precision of how well the sampled region/area was represented at the same position of corresponding samples of the same period.

Score	Sample description
1 or **2**	The region/area of interest was absent (1) or largely absent (2) and thus not collected.
3	The region/area of interest was not complete but was of suitable quality to collect.
4	The region/area of interest was largely intact but was not histologically verified or could not be collected at precisely the same position from which the corresponding contralateral sample was collected.
5	The region/area of interest was fully intact, verified by gross inspection or Nissl staining (NCX areas), and collected at precisely the same position as corresponding samples of the same period.

3.4.4. Tissue pulverization

To ensure proper representation of the region of interest, frozen tissue samples were pulverized in liquid nitrogen using a ceramic mortar and pestle (Fisher Scientific, cat# 12-961C and 12-961-5C). Pulverized samples were transferred to chilled wide-mouth cryogenic vials (Nalgene, cat# 03-337-7B) and stored at -80 ºC until used for RNA extraction.

4. DNA Isolation and Genotyping Data Analyses

4.1. DNA extraction and genotyping

For genotyping analysis, up to 25 mg of brain tissue, usually collected from the CBC, was homogenized using a bead mill homogenizer (Bullet Blender, Next Advance) and lysed in Buffer ATL (Qiagen) at 56 °C for 3–4 h. Genomic DNA was isolated using a non-phenolic procedure (DNeasy Blood & Tissue Kit, Qiagen) followed by proteinase K and RNase A treatment (Qiagen). Optical density values of extracted DNA were measured using a NanoDrop (Thermo Scientific) and PicoGreen dsDNA assay kit (Invitrogen). DNA integrity was confirmed by agarose gel electrophoresis. Illumina Omni-2.5 million SNP arrays were used for genotyping analysis. DNA samples were processed at the Yale Center for Genome Analysis according to the Infinium HD Assay Super, Automated Protocol for Human Omni 2.5-Quad Bead Chip (Illumina).

4.2. Copy number variation (CNV) analysis and genomic quality control

All SNP-arrays were scanned using the Illumina iScan system. The intensity files were analysed using Illumina GenomeStudio v2010.2 software. Sex of each sample was determined from the SNP genotyping results using GenomeStudio to confirm the metadata of each sample. Two algorithms were used to detect CNV from SNP intensity data. The cnvPartition algorithm in GenomeStudio was used to detect CNV. The measurement of B allele frequency and $\log_{10}$-transformed R ratio of all SNPs were exported to the program PennCNV to confirm CNVs. The two sets of results were compared and only CNVs detected by both algorithms were included in the final results (Supplementary Fig. 4 and Supplementary Table 2). Only specimens with no signs of chromosomal or large-scale genomic abnormalities were considered for the study.

4.3. Corroborating and refining ethnic background from genotypes

Ethnicity of donors was reported by next of kin. However, in the majority of prenatal and some postnatal cases the ethnicity of the father was not available. For this reason, the ethnic background was corroborated and refined by comparing the result of SNP analysis of each individual to SNP data available in HapMap III. The whole allele frequency dataset of the following ethnic populations was downloaded from HapMap III (ftp://ftp.ncbi.nlm.nih.gov/hapmap/frequencies/2010-08_phaseII+III/): (1) Utah residents of Eastern and Western European descent (CEU); (2) Toscani in Italy (TSI); (3) Yoruba, in Ibadan, Nigeria (YRI); (4) African ancestry in Southwest USA (ASW); (5) Luhya in Webuye, Kenya (LWK); (6) Maasai in Kinyawa, Kenya (MKK); (7) Chinese in metropolitan Denver, Colorado (CHD); (8) Japanese in Tokyo, Japan (JPT); (9) Mexican ancestry in Los Angeles, California (MEX) and (10) Gujarati Indians in Houston, Texas (GIH).

A group of SNPs frequently expressed in some populations but rarely in others was first selected. The maximum allele frequency and minimum allele frequency in the 10 populations were calculated for each SNP. Population specific SNPs were defined as those for which the difference between the maximum and minimum allele frequency was greater than 0.6. These population-specific SNPs were cross-referenced against the SNPs identified by genotyping of our samples. Only the common set of SNPs was used in the following calculation.

The common set of SNPs is designated as S_i, where i is a variable value that represents a specific SNP. The genotype G_i of SNP S_i could be AA, AB or BB, where A and B are two alleles for the SNP. The

populations are designated as P_j, where j is a value of 1 through 10 that represents a specific ethnicity, as defined above. The A-allele frequency of SNP S_i within population P_j is f_{ij}. For any individual in a specific population P_j, the probability of having the genotype G_i at SNP S_i is:

$$p_{ij} = \begin{cases} f_{ij} * f_{ij} & \text{if } G_i = AA \\ 2 * f_{ij} * (1 - f_{ij}) & \text{if } G_i = AB \\ (1 - f_{ij}) * (1 - f_{ij}) & \text{if } G_i = BB \end{cases}$$

The $\log_{10}$-transformed likelihood function (L_j) that describes the probability of any individual from population P_j having exactly the same genotypes as the analyzed samples at a specific set of SNPs would be:

$$\log_{10}(L_j) = \log_{10}\left[\prod_{i=1}^{n} p_{ij}\right]$$
$$= \sum_{i=1}^{n} \log_{10}(p_{ij}).$$

Therefore, the $\log_{10}$-transformed likelihood ratio for population P_j compared to the reference population P_0 is:

$$\log_{10}(L_j/L_o) = \sum_{i=1}^{n} \left[\log_{10}(p_{ij}) - \log_{10}(p_{i0})\right]$$

The likelihood ratio for each population was used to assign ethnicity. "European Ancestry" was assigned to samples for which the two highest-score populations were CEU and TSI. "African Ancestry" was assigned if the four highest-score populations were YRI, ASW, LWK and MKK. "Asian Ancestry" was assigned if the three highest-score populations were JPT, CHD, and GIH. "Hispanic Ancestry" was assigned if the highest-score population was MEX. "Mixed" was assigned as the default ancestry if none of the above conditions could be met.

5. RNA Isolation, Exon Array Processing, and Quality Assessment

5.1. RNA extraction
A bead mill homogenizer (Bullet Blender, Next Advance) was used to lyse the pulverized tissue. Each pulverized tissue sample was transferred to a chilled safe-lock microcentrifuge tube (Eppendorf). A mass of chilled stainless steel beads (Next Advance, cat# SSB14B) equal to the mass of the tissue was added to the tube. Two volumes of Buffer RLT Plus (Qiagen) were added to the tissue and beads. Samples were mixed in the Bullet Blender for 1 min at a speed of six. Samples were visually inspected to confirm desired homogenization and then incubated at 37 °C for 5 min. Buffer RLT Plus was added up to 0.6 ml, and samples were mixed in the Bullet Blender for 1 min. Total RNA was extracted using a non-phenolic procedure (RNeasy Plus Mini Kit, Qiagen), followed by DNase treatment (TURBO DNase, Ambion) as per manufacturers' instructions. Optical density values of extracted RNA were measured using NanoDrop (Thermo Scientific) to confirm an A_{260}:A_{280} ratio above 1.9. RIN was determined for each sample using Bioanalyzer RNA 6000 Nano Kit or Bioanalyzer RNA 6000 Pico Kit (Agilent), depending upon the total amount of RNA.

5.2. Exon array hybridization

Exon array hybridizations were performed at the Yale Center for Genome Analysis and at Gene Logic Inc. (Gaithersburg, MD). Reverse transcription (RT) was performed to generate cDNA from total RNA using RT primers designed using an oligonucleotide matching algorithm. For the selective cDNA synthesis, the Ambion WT Expression kit (Ambion) was used in combination with the GenechipWT Terminal Labeling and Controls Kit (Affymetrix) for target preparation, according to manufacturers' recommendations. PolyA controls were added to the input RNA to measure efficiency of target amplification. Fragmented and labelled second cycle cDNA (5.5 μg) was added to a hybridization cocktail prior to loading of 200 μl onto individual Affymetrix Human Exon 1.0 ST arrays, which features comprehensive coverage of the human genome, with 1.4 million probe sets that assay exon expression across the entire transcript. Microarrays were hybridized at 45 °C for 16–24 hours, washed and stained using an Affymetrix FS450 fluidics station, according to manufacturer recommendations. Microarrays were scanned on a GeneChip Scanner 3000 and visually inspected for hybridization artifacts. The raw image files (.DAT files) were analysed using Affymetrix GeneChip Operating Software to generate .CEL files.

5.3. Exon array quality assessments

Several quality control measures were implemented throughout microarray sample preparation and transcriptome data generation steps (Supplementary Fig. 5) to reduce errors due to spatial artifacts on the chips, technical differences between chips in probe saturation, differences in the intensity of the probes along the 5'to 3' gradient of genes, or due to other unaccounted batch effects. First, an idealized reference chip was constructed for all arrays hybridized at each facility by computing the 15% trimmed mean of the $\log_2$-transformed probe intensities for each of the 5.5 million perfect match probes across all arrays. Spatial artifacts were defined as severe non-random spatial patterns in the ratios of intensities of probes on one chip relative to corresponding probes on the ideal reference chip; such artifacts are believed to arise from non-uniform hybridization conditions across the surface of an array. By design, microarray probes are randomly distributed across an array to avoid spatial biases, i.e., probes that represent adjacent regions on the genome are not located physically adjacent on an array. Consequently, in the absence of spatial artifacts due to error sources in pre-processing steps, one would expect a random pattern of probes with higher or lower intensities relative to the reference chip. Supplementary Fig. 6 shows ratio intensity plots for arrays with severe spatial artifacts.

In addition, exon array hybridization uniformity was estimated by gene expression uniformity from 5'-end to 3'-end (Supplementary Fig. 6). Samples with altered hybridization uniformity and microarrays displaying regional biases or other spatial artifacts were excluded/or re-tested. Low-quality RNA samples identified by these quality control measures were excluded from further analysis (N=53).

To evaluate technical reproducibility and the possibility of batch effects, four identical samples were processed at different testing centers. To evaluate biological reproducibility, we calculated the correlations between the same regions collected from different individuals of the same period. The correlations were high for both technical (Spearman correlation, $r^2 = 0.967$; N=8) and biological replicates ($r^2 = 0.926$; 1,340 total), reinforcing the validity of our approach and data.

The impact of confounding factors on the quantity, quality, and transcriptional profile was controlled by computing correlations between the number of expressed gene and the following variables: PMI, pH, RIN, and DS. Of these factors, only PMI and RIN showed a weak anticorrelation and correlation, respectively, with the number of expressed genes (Spearman correlation, $r = -0.382$ and 0.278, respectively; Supplementary Fig. 12), indicating that the collected tissue samples were suitable for profiling the transcriptome.

5.4. Detection of outliers

We used several approaches to identify outliers based on processed exon array samples. First, we performed average-linkage hierarchical clustering of all samples corresponding to different regions using 1-correlation as a distance and related them to the following variables: age, sex, ethnicity, PMI, DS, RIN, and the array processing site. For the NCX, the expression and the RIN of areas from the same hemisphere of an individual were averaged. Hierarchical clustering revealed notable clustering of the samples based on age and regions (Supplementary Fig. 8). Out of 1,346 samples, 5 samples from the same brain were found to be outliers based on hierarchical clustering and subsequently removed from further analyses.

Second, the averaged Spearman correlation coefficient of a given brain region/NCX area was calculated for each period, and those samples with values outside 3 standard deviations (SDs) were considered as outliers. One sample was found to be an outlier and subsequently removed from the downstream analysis. Finally, a total of 1,340 exon microarray samples from 57 brains passed the quality control steps and were included in this study (Supplementary Tables 3 and 4).

5.5. Exon array data pre-processing

Partek Genomics Suite version 6.5 (Partek Incorporated, St. Louis, MO, USA) was used to normalize raw exon array data and to summarize expression of the probe set and transcript cluster. Affymetrix CEL files that passed QC analyses were imported into Partek Genomics Suite using the default Partek settings: RMA background correction[58], quantile normalization, mean probe set summarization, and $\log_2$-transformation. All analyses reported used only the core and unique probe sets, which hybridize to unique genomic positions and are based on well-curated RefSeq (www.ncbi.nlm.nih.gov) and Ensembl transcripts (www.ensembl.org) as well as GenBank transcripts (http://www.ncbi.nlm.nih.gov/genbank/) annotated as complete protein-coding sequences. A total of 17,565 mainly protein-coding genes were surveyed.

Datasets were annotated according to the UCSC human genome hg19 reference sequence (http://genome.ucsc.edu/cgi-bin/hgGateway). 105,271 core probes (within 62,448 probe sets out of 230,918 core probe sets) contained SNPs defined in the probe group file HuEx-1_0-st-v2.r2-SNPs-Excluded.pgf provided by Affymetrix, which is based on the dbSNP database (version 129, April 2008) and SNPinprobe_1.0 database. As previously observed[59,60], inclusion of SNP-containing probes can affect the hybridization of the probes and thus produce misleading signal intensity values. To test the effects of these SNP-containing probes, the whole-transcript and probe set signal intensity were evaluated twice, with one evaluation excluding SNP-containing probe sets by filtering out the affected probes that hybridized to regions with common SNPs (minor allele frequency (MAF) $\geq$ 0.05). The Pearson correlation analysis was performed to compare whole-transcript and probe set signal intensities of the data with and without SNP-containing probe sets. Most of the correlation coefficients (98.8%) for all 1,340 samples were within the range of 0.980-0.995 for whole-transcript and 0.975-0.995 for probe sets, suggesting that SNP-containing probe sets have a very minimal effect on measured signal intensity levels (Supplementary Fig. 7). Nevertheless, we removed SNP-containing probe sets during the normalization step in the Partek program to be control for SNP-related confounding effects. The median of all individual probe sets of one transcript cluster was used as the estimate of gene expression values. To filter out low expression signals (including noise or poorly hybridized probes), which may lead to false positives, detection above background (DABG) *P*-values of exon probe sets and transcript clusters were calculated using Affymetrix power tools (APT, http://www.affymetrix.com/partners_programs/programs/developer/tools/powertools.affx).

6. Exon Array Data Analysis

6.1. Gene-level analysis

The signal intensity for all core and unique probes within a probe set were averaged to obtain an expression value for the probe set. The median of all probe sets within one gene (transcript cluster) was used as the estimate of gene expression. Since most exons are represented by only one probe set, we used the probe set signal intensity as synonym of exon expression level, unless explicitly mentioned. To reduce the noise in the dataset and the false positives in the following differentially expressed genes and alternative exon usage investigations, we excluded genes with a $\log_2$-transformed expression value <6 in all 1,340 samples. We defined an "expressed" gene as a gene with a $\log_2$-transformed expression value ≥6 in at least one sample and DABG P<0.01 in one or more of the sampled brain regions or NCX areas during at least one time period. To demonstrate the underlying distribution of the data using these criteria to define expression, the signal intensity distribution plots of expressed, non-expressed gene, and intronic controls (designed from the intron regions of a set of housekeeping genes) are shown in Supplementary Figure 9.

6.2. Multi-dimensional scaling (MDS)

MDS analysis was performed by generating expression vector for all expressed genes for each of the analyzed samples. We calculated the Euclidean distance between each pair of vectors to obtain a distance matrix with dimension 1,340 x 1,340. The R function *isoMDS* was used to calculate two-dimensional MDS. The returned two vectors were used as coordinates x and y for each of the 1,340 samples to make a scatter plot in a 2-dimensional plane. The 1,340 data points, each representing one tissue/array sample, were plotted and colored according to the phenotype of the samples, such as time period, brain region, sex, ethnicity, or donor's code (Supplementary Fig. 10).

6.3. Principal component analysis (PCA)

PCA from prcomp package and three-dimensional view from rgl package, both retrieved from R (http://www.r-project.org/), were used to visualize the relatedness of all 1,340 microarray samples. Our results show that the samples were clustered by developmental periods and functional regions. Three different directional views are shown in Supplementary Fig. 11.

6.4. Identification of spatial and temporal DEX genes

Analysis of variance (ANOVA) was used to identify differentially expressed (DEX) genes across all brain regions of interest and during all periods (1-15). Genes that were differentially expressed in at least one brain region or NCX area were identified as spatial DEX based on ANOVA by using a brain region/NCX area as an ANOVA factor. Genes differentially expressed in at least one time period were identified as temporal DEX based on ANOVA using a period as a factor. In order to exclude the possibility that variation in PMI and RIN might influence the detection of DEX, we included PMI and RIN as technical covariates within our ANOVA model of differential expression. We found that RIN accounted for a mean variance of 2.16 in the spatial analysis for all genes, which was 8% of the mean total variance across genes, and a variance of 1.02 in the temporal analysis, which was 3% of the mean total variance of that analysis. We found that PMI accounted for a mean variance of 1.89 in the spatial analysis, which was 8% of the mean total variance, and a variance of 0.33 in the temporal analysis, which was 1% of the mean total variance of that analysis. Resulting P-values from ANOVA were corrected for multiple comparisons using the Benjamini and Hochberg false discovery rate (FDR) method[62]. A conservative statistical threshold (FDR <0.01 and minimum fold difference >2 between brain regions/areas or periods) was used to identify DEX genes. Genes that were not significantly expressed above background were excluded from ANOVA tests.

To ensure that our results are robust and are not unduly influenced by any particular sample, we used a five-fold jackknife procedure. Samples were split into 5 random groups and re-analyzed for DEX genes 5

times by leaving out one group in each cycle of analysis. The genes from each of the five re-sampling showed a high rate of overlap with the genes obtained from the whole dataset (Supplementary Fig.13).

To identify spatially DEX genes that were selectively highly enriched or restricted in only one of the regions, irrespective of their temporal regulation, we used a combination of t-test and fold difference analyses. We limited this spatial DEX analysis to periods 3-15, when regions/areas of interest are defined using equivalent criteria and can be consistently followed across time. We used a sliding-window algorithm to detect regionally enriched genes within a group of sequential periods. The window size was set as 5, scanning periods 3-7, 4-8, 5-9, 6-10, 7-11, 8-12, 9-13, 10-14, 11-15. For each window, a two-sample t-test was applied to determine if the expression level of a gene in one selected region was significantly different from the expression level in the samples from other regions. To calculate the fold difference in averaged signal intensity, two regions were used: the region of interest and, from the remaining regions, the one that had the highest averaged expression value. The *P*-values from the t-tests were transformed to FDR using the Benjamini and Hochberg method. A gene with FDR <0.01 and minimum fold difference >2 in a given window was considered to be highly enriched in or restricted to one region. If the window contained both prenatal and postnatal periods or both postnatal and adult periods, a post-hoc group assignment analysis was performed in order to determine if the DEX genes should be assigned to one or both of the developmental groups. We calculated the fold difference attributed to the two periods bordering each side of the developmental groups (6-7 and 8-9 for prenatal-postnatal group; 11-12 and 13-14 for postnatal adult group). If the fold difference was greater than 1.5, the DEX gene was assigned to that developmental group, resulting in either one or both groups being assigned the gene.

6.5. Analysis of DEU

To identify expressed genes that exhibit differential exon usage (DEU) across all regions of interest and during all periods, we used a splicing ANOVA method and a splicing index (SI) algorithm[61]. Normalized intensities (NI) were calculated as the expression of an individual exon relative to the expression of the gene. Splicing index was defined as the fold difference of the normalized intensity of exons between two groups (periods and/or regions). Both spatial DEU and temporal DEU were analysed. For spatial DEU, the ANOVA factor is set as the brain region/NCX area. All periods were tested and the maximum of splicing indexes among regions/areas was calculated. For temporal DEU, the ANOVA factor is set as the period. Sixteen regions/areas were tested, and the maximum of splicing indexes among periods was calculated. We included PMI and RIN as technical covariates within our ANOVA models. Resulting *P*-values from ANOVA were corrected for multiple comparisons using the Benjamini and Hochberg FDR method[62]. Stringent criteria (FDR <0.01 and maximum splicing index >2) were used, and exons expressed at low levels or with low variance (standard deviation of exon expression level <0.5 in all samples, which indicates they are very likely to be saturated in all samples) were excluded.

To test the robustness of our DEU, we used a five-fold jackknife procedure. Samples were split into 5 random groups and re-analyzed for DEU genes 5 times by leaving out one group in each cycle of analysis. The exons from each of the five re-sampling showed a high rate of overlap with the exons obtained from the whole dataset (Supplementary Fig.13). These analyses indicate that our findings are robust and did not depend on any particular sample.

6.6. Identification of sex-bias in DEX and DEU

Sex-biased DEX genes were identified by the combination of a sliding window algorithm, two-sample t-test, and fold difference analysis. The sliding-window algorithm was used to detect gene expression differences between males and females within a group of sequential periods. The window size was set as 5, which

ensured adequate representation of both sexes, and periods 2-6, 3-7, 4-8, 5-9, 6-10, 7-11, 8-12, 9-13, 10-14, 11-15 were scanned. For each window, a two-sample t-test was applied to determine if the expression level of a gene in male samples was significantly different from the expression level in female samples in the same region. The *P*-values from the t-tests were transformed to FDR using the Benjamini and Hochberg method[62]. For each gene, the fold difference (log$_2$-transformed) between male and female samples in each region was also calculated. An FDR <0.01 and 2-fold difference were used as a cutoff to identify genes that are DEX between males and females in each window. If the window contained both prenatal and postnatal periods or both postnatal and adult periods, a post-hoc group assignment analysis was performed in order to determine if the differentially expressed genes should be assigned to one or both of the developmental groups. We calculated the fold difference attributed to the two periods bordering each side of the developmental groups (6-7 and 8-9 for prenatal-postnatal group; 11-12 and 13-14 for postnatal-adult group). If the fold difference was greater than 1.5, the differentially expressed gene was assigned to that developmental group, resulting in either one or both groups being assigned the gene (Supplementary Table 7).

Sex-biased DEU was investigated by splicing index and two-sample t-test. Each exon cluster was normalized by dividing its expression by the gene-level expression to yield a normalized intensity. The splicing index was then calculated as a "fold change" between the normalized levels of each exon cluster from male and female samples. As in the sex-biased DEX analysis, the sliding window algorithm was also used. An FDR cutoff of 0.01 and 2-fold difference were used for sex-biased DEU (Supplementary Table 8). Exon clusters that were expressed at low levels (log$_2$ intensity <6) or with low variance (standard deviation of exon expression level <0.5 in all 1,340 samples were excluded. Y chromosome genes were also excluded from the analysis.

Analyses of sex-bias in DEX and DEU were performed without considering PMI and RIN as covariates because we did not find any significant differences of PMI and RIN values between female and male tissue samples. PMI, 12.01 ± 9.01 (N=31, mean ± s.d.) for males and 11.4 ± 8.09 (N=26, mean ± s.d.) for females; RIN, 8.86 ± 0.87 for males and 8.79 ± 0.99 for females.

6.7. Weighted gene co-expression network analysis

6.7.1. Dataset filtering
Only samples from periods 3–15 were included in the weighted gene co-expression network analysis (WGCNA). During these periods, brain regions and NCX areas are well-defined using equivalent criteria and can be consistently followed across time. NCX areas were not present in periods 1 and 2.

6.7.2. Network construction and module detection
To reduce noise, only genes with log$_2$-intensity values greater than 6 in at least one sample and a coefficient of variance greater than 0.08 were used. A total of 9,093 genes fit these criteria. Signed weighted gene co-expression network analysis was performed using WGCNA R package[65]. General information about network analysis methodology and WGCNA software is available at www.genetics.ucla.edu/labs/horvath/CoexpressionNetwork. Pairwise Pearson correlation coefficients were calculated for all genes selected. The resulting Pearson correlation matrix was transformed into a matrix of connection strengths (an adjacency matrix) using a power function (connection strength = $(\frac{1+correlation}{2})^{\beta}$), which was then converted to a topological overlap matrix. WGCNA seeks to identify modules of densely interconnected genes by hierarchical clustering based on topological overlap [62]. The first principal component (PC1) of each module was calculated and smoothed by smoothing spline against

$\log_{10}$ [days postconception]. The top 50 genes expressing the highest within module connectivity were selected and exported to VisANT for network visualization[66].

6.7.3. Module filtering

The grey module consisted of genes not assigned to any of the module was removed (Fig. 4). To check the effects of RIN, PMI, dissection, and pH on module identification, we constructed a linear model $PC1_i = age_i + region_i + sex_i + RIN_i + PMI_i + pH_i + DS_i$ (where $PC1_i$, age_i, $region_i$, sex_i, RIN_i, PMI_i, pH_i, DS_i, are the first principle component, $\log_{10}$ [days postconception], sex, RIN, PMI, pH and DS of sample i, respectively). ANOVA was then performed, and the coefficient of determination (r^2) and *P*-value of each factor was calculated. The modules with r^2 of any factor greater than 0.1 and r^2 of any confounder (RIN, PMI, pH and DS) larger than the largest r^2 of the main factors (age, region and sex) were considered as modules corresponding to confounders. Six modules were detected as confounder-related modules and removed from further analysis (Supplementary Table 11).

6.7.4. Comparison of modules with transcriptional profiling of neurobiological categories

To gain insight into module functions, we compared each module with our manually created functional gene lists for specific neurobiological categories. The correlation between module eigengene (the first principle component of module expression) and the PC1 summarization of each functional gene list was calculated and listed in Supplementary Table 10.

6.8. Gene ontology (GO) enrichment analysis

Functional enrichment was assessed using DAVID Bioinformatics Resources 6.7[63,64] (http://david.abcc.ncifcrf.gov/).

6.9. Creation of gene lists and transcriptional profiling of neurobiological categories

We manually curated lists of genes functionally related to specific neurodevelopmental processes, neural cell types, and neurotransmitter systems, by selecting individual genes or a small group of genes from the existing gene ontology (GO) database (http://www.geneontology.org/) whose functions, and thus expressions, have been most closely associated with specific neurobiological category based on published data from model organisms and human medical genetics (Supplementary Table 12 and data available on the website: www.humanbraintranscriptome.org). We expected that the selected genes or gene group might accurately reflect the trajectories of neurobiological processes in neurodevelopment. To summarize the principle gene expression profile of each category, PCA was performed. The resulting PC1 was plotted against logarithmic age in days, and a smooth curve was fitted by smoothing spline to display the developmental trajectories. For categories with only one gene, the expression level was used as PC1.

We also curated gene lists for neurotransmitter systems by compiling genes encoding critical enzymes for transmitter synthesis and receptor subunits. To compare the spatio-temporal patterns of genes in the same group, we plotted genes in each group individually and fitted the individual gene expression pattern by smoothing spline (Supplementary Table 12 and data available on the website: www.humanbraintranscriptome.org).

To test the accuracy of this strategy, three gene expression trajectories (*DCX*, dendrite development genes, synapse development genes) were compared with independently generated, non-transcriptome datasets for DCX-positive cell density, synaptic density, and the number of basal dendrites in the corresponding brain regions/areas, respectively (Figure 5). The independent data were scaled by $\frac{x-\mu}{\sigma}$. μ and σ are the mean and the standard deviation of values, respectively, corresponding to the time periods for which both our gene expression and the independently generated data were available. Our scaled gene expression data were used to

generate a spline curve, and the predicted values on this curve were calculated corresponding to available time points of previously generated independent data on DCX, dendrite development, and synaptogenesis, which used samples at different time points but within our defined periods. We then calculated the correlation coefficient between our predicted data and the actual values.

To compare the developmental trajectories for cell proliferation, neuron migration (*DCX*), dendrite development, myelination and synapse development gene markers, PC1 of each group was subjected to smoothing spline curve fitting. The fitted value $\hat{y}_i$ was then scaled to 0 to 1. The range of fitted vector $\hat{Y}$ is set to 1, and the scaled values were calculated as $z_i = (\hat{y}_i - \min(\hat{Y}))/ \operatorname{range}(\hat{Y})$. The scaled values were then plotted to represent the trajectory of each group with a measure of the percentage of changes (Fig. 5).

To select genes potentially associated with the neurodevelopmental processes and neural cell types, the top 100 genes positively correlated with PC1 of each functional gene list were presented in Supplementary Tables 13 and 14.

6.10. Expression trajectories and gene correlations for ASD- and schizophrenia-associated genes

A list of genes commonly associated with autism spectrum disorders (ASD) was obtained from recently published reviews[10,67]: and relevant databases (www.g2conline.org). A list of genes commonly associated with schizophrenia was obtained from meta-analysis list[68] and relevant databases (www.szgene.org/topresults.asp; www.g2conline.org). In the szgene database list, genes with an assigned overall grade A, which indicates the highest/strictest association, were included in the analysis. Lists of genes for the two disorders and other correlated transcripts are provided in Supplementary Tables 15 and 16.

To generate representations of the dynamics in spatio-temporal expression of representative genes (*CNTNAP2, MET, NLGN4X, NRGN*), a heat map matrix was created for each of these genes according to the following method. For each combination of developmental period and brain region/area, the $\log_2$-transformed expression level values of related samples were averaged to obtain a single value of expression level at the specific period and specific brain region/NCX area. All of these average values were collected into a data matrix, where each row represented one brain region/area and each column represents one period. After the matrix was created, a heat map plot was created using R function 'heatmap.2' in package 'gplots' (Supplementary Figure 25).

The top 50 genes, ranked by their correlation with individual genes previously associated with ASD and schizophrenia, are presented in Supplementary Tables 15 and 16. Genes with the highest correlation to the disease-related genes were grouped, and subjected to functional enrichment assessment using DAVID Bioinformatics Resources 6.7 (http://david.abcc.ncifcrf.gov/).

7. Transcriptome Validation Methods

7.1. Quantitative real time RT-PCR and semi-quantitative RT-PCR

An aliquot of the total RNA that was previously extracted from each brain region was used for secondary validation through real-time PCR analysis. One µg of total RNA was used for cDNA synthesis using SuperScript III First-strand synthesis Supermix (Invitrogen) and subsequently diluted with nuclease-free water to 1 ng/µl cDNA. Gene-specific high-melting temperature primers for genes of interest were designed using NCBI/Primer-BLAST (http://www.ncbi.nlm.nih.gov/tools/primer-blast/) and expressed sequence information obtained from GenBank (NCBI). PCR reactions were conducted on an ABI 7900 Sequence Detection System (Applied Biosystems) using a hot start SYBR-green based method (Fast SYBR Green Master Mix, ABI) followed by melting curve analysis to verify specificity of the product. The Ct value (cycle number at threshold) was used to calculate the relative amount of mRNA molecules. The Ct value of each target gene

was normalized by the subtraction of the Ct value from housekeeping genes to obtain the Δ Ct value. The relative gene expression level was shown as $2^{-\Delta Ct}$ or $-\Delta$ Ct. All human genes of interest were normalized to the housekeeping gene *GAPDH*.

Semi-quantitative RT-PCR was performed using the same template and hot start Taq DNA polymerase (Qiagen) under the following conditions: activation at 95 ºC for 10 min, followed by 30–40 cycles at 94 °C for 30 sec, 56 °C for 30 sec, 72 ºC for 60 sec, and extension at 72 ºC for 10 min. The cycling conditions were chosen so that none of the templates analyzed reached a plateau at the end of the thermal cycling, i.e., they were in the exponential phase of amplification. PCR products were separated on a 2% agarose gel and photographed using UV illumination to visualize ethidium bromide staining. Images were inverted in Adobe Photoshop.

7.2. List of PCR primers used in this study

Gene	Forward primer (5' ->3')	Reverse primer (5' ->3')
GAPDH	TTCTTTTGCGTCGCCAGCCGA	GTGACCAGGCGCCCAATACGA
HDAC2	TGGCCGGGGAGCCCATGG	GGCAGTGGCTTTATGGGGCCTATAT
TF	CGGAAGATGAGGCTCGCCGT	TGCTCCGACACTGCACACCA
RGS16	TGGCAAGTTCGAGTGGGGCA	GGAAAGCGTGGAAGGCAGCCA
GABRA6	TTTGGGCCCGTGTCAGATGTGG	GGTGTCAGGCGTCCAGATTTTACTG
RGS9	GGACTACGGCCTGGACCGAGT	ACAATCCCTCCCAGGGACACAGA
PCDH11Y	GGCCTGCCCCTTGGCTATCC	GGCCTCTTCCACAGTTGGTTGAACA
ANKRD32a	TGTTTGTTGCAGAGGCAGTC	GACCCAAGCACACCAGTTTT
ANKRD32b	ACTAGGGGAGACAATGCCTGT	CCCACCAATCCATACTGCTT
NLGN4X (exon 7)	TGAGACTCACAGGCGCCCCA	CGTGTGCCTGCAGCGACTCA
NLGN4X (3'UTR)	CCCTCTGCCCTACCCGCTCA	GCCGGGATGGGATGACTGCC
GLIPR1L2	CCTGGCAGTAGGGGGCGTTT	TCCCAAGTCATGAAGCGCAAGTTAG
Rpl32	CAACATCGGTTATGGGAGCAACA	TGACATTGTGGACCAGGAACTT
Ankrd32a	CAGGGCCCCACTAGTACGTGC	AGCTCTGGCCGACCTTCTGCT
Ankrd32b	GGCATGGGTCCAGACCTTCTAGTT	GCGTCCAGCCAGCATTGTCTT

IGF2	Hs00171254_m1 (Applied Biosystems)	
GAPDH	Hs99999905_m1 (Applied Biosystems)	

7.3. Immunohistochemistry and histochemistry

For neuropathological evaluation and validation studies, brain tissue samples were fixed in 4% PFA for 2–3 days at 4 °C. Following fixation, tissue was cryoprotected in graded sucrose solutions (up to 30%) at 4 °C, then frozen at -40 °C in isopentane/dry ice, and stored at -80 °C. Alternatively, fixed tissue samples were paraffin-embedded for routine neuropathological evaluations.

Frozen tissue samples were cut at 60 μm using a Leica CM3050S cryostat and either mounted onto Superfrost/Plus slides (Fisher Scientific Co.) or used free-floating. Tissue sections were incubated in 1% hydrogen peroxide/PBS to quench endogenous peroxidase activity. Sections were washed in PBS (3 x 15 min) and incubated in blocking solution containing 5% (v/v) normal donkey serum (Jackson ImmunoResearch Laboratories), 1% (w/v) bovine serum albumin, and 0.4% (v/v) Triton X-100 in PBS for 1 h at room temperature. Primary antibodies were diluted in blocking solution and incubated with tissues sections

overnight at 4 °C. Sections were washed with PBS (3 x 15 min) prior to being incubated with the appropriate biotinylated secondary antibodies (Jackson ImmunoResearch Labs) for 1.5 h at room temperature. All secondary antibodies were raised in donkey and diluted at 1:200 in blocking solution. Sections were subsequently washed in PBS and incubated with avidin-biotin-peroxidase complex (Vectastain ABC Elite kit; Vector Laboratories) for 1 h at room temperature. Finally, sections were washed in PBS (3 x 15 min) and signals were developed using a DAB peroxidase substrate kit according to the manufacturer's protocol (Vector Laboratories). Following washes in PBS, sections were mounted on Superfrost Plus charged slides, dried, dehydrated, and cover slipped with Permount (Fisher Scientific Co.). Sections were digitized using ScanScope scanner (Aperio). Digitized images were assembled in Adobe Photoshop and Illustrator.

NADPH-diaphorase histochemistry was performed as previously described[69].

8. Dissection of the Mouse Neocortex

We performed qRT-PCR in orthologous areas of the mouse NCX at equivalent developmental periods using a mathematical model to translate neurodevelopmental time across mammalian species[70] (www.translatingtime.net). For analysis of mouse *Ankrd32* by qRT-PCR, CD1 mice were obtained from Charles River Laboratories. Mice were sacrificed according to institutional regulations. Brains from embryonic day (E) 15, postnatal day (P) 3 and adult mice (3 brains per period) were dissected either fresh in cold PBS or after storage of the whole brain in RNA*later* reagent (Qiagen). Dissected regions were sampled according to the "Prenatal Mouse Brain Atlas" (for E15 mouse brain) and "Atlas of the Developing Mouse brain" (for P3 and adult mouse brain)[71,72]. The following regions were dissected:

E15:
- MFC – sampled from medial part of the frontal cortex.
- DLFC – sampled from dorsolateral part of frontal cortex (containing prospective primary motor cortex).
- S1C – sampled from anterior part of parietal cortex.
- A1C – sampled from prospective primary auditory cortex (upper part of prospective temporal cortex).
- V1C – sampled from occipital part of the hemisphere.

P3 and **adult**:
- OFC – sampled from orbital part of the frontal cortex after removal of olfactory bulb (containing VO and LO areas according to Paxinos et al.).
- MFC – sampled from medial part of the frontal cortex (containing PrL and IL areas according to Paxinos et al.[71]).
- M1C – sampled form the dorsal part of the frontal cortex (containing M1 and M2 areas according to Paxinos et al.).
- S1C – sampled from the rostral part of the parietal cortex (containing all S1 area subdivisions according to Paxinos et al.).
- A1C – sampled from the upper part of the temporal cortex (containing AuD, Au1 and AuV areas according to Paxinos et al.).
- V1C – sampled from the occipital part of the hemisphere (containing V1, V2ML, and V2L areas according to Paxinos et al.).

RNA extraction of P3 and adult samples was performed following the same protocol used for human tissue samples (see Supplementary Information 5.1). Due to the small amount of tissue for E15 samples, a Trizol (Invitrogen) extraction protocol was performed according to manufacturer's instructions. Eighty ng of total RNA was used for cDNA synthesis, and quantitative RT-PCR was performed and analyzed as the same method with human brain samples. Ct values were normalized to the housekeeping gene *Rpl32*. Three technical replicates were performed on each sample.

9. Expression Quantitative Trait Loci Analysis

The genotyping results consisted of 2.5 million SNPs for each of 57 brains using Illumina Omni-2.5 SNP arrays. We used PLINK to calculate the minor allele frequency (MAF), Hardy-Weinberg p-value and SNP-wise call rate for each SNP. The eQTL analysis was restricted to 890,000 SNPs that had MAF >0.1, Hardy-Weinberg p-value >0.05, and SNP-wise call rate greater than 0.99 in order to reduce genotyping errors and increase statistical power. The analysis was further restricted to SNPs within 10 kb of the transcription start or stop sites of the 15,132 expressed genes.

The expression data in 11 NCX areas were averaged to get a single expression value in NCX for each gene, and *cis*-eQTL analysis was conducted separately for each region as described below. We adjusted for other non-genetic factors impacting gene expression measures in two ways. First, our phenotype was the expression level relative to the average developmental trend for each gene (see below); this allowed us to focus on the individual variation independently of the developmental trends. Second, we included possible confounding factors as covariates in our linear model for relative expression; these covariates included RIN, PMI, sex, the first two principal components of the global transcriptome, and ethnicity.

In order to compare individual differences in single gene expression across developmental time points, we adjusted the expression values as follows. For each gene, we sorted the expression values in 57 brains according to their age and fitted a smooth function (computed by local regression or LOWESS) to obtain the average expression levels over development stages. We calculated a relative expression level by subtracting the value of this trend curve from the normalized individual gene expression value.

After separating genes and SNPs by chromosome, PLINK was used to conduct a quick scanning for possible associations between all genes and SNPs near the beginning and end of the gene as described above with the following arguments: 'plink --file myfile --pheno expression.txt --all-pheno --assoc --pfilter 1e-3 '. Using these phenotypes, we ran linear regression using PLINK with following settings: "plink --file selectfile --pheno select_expression.tx --sex --all-pheno --covar covariants.csv --covar-name PC1, PC2, PMI, RIN, Cauc, Afric, Asia, Hisp --linear --pfilter 1e-3".

A conservative two-level strategy was applied for multi-test correction. We performed a Bonferroni correction for all tests involving the same gene to obtain a gene-wise adjusted p-value for the SNP with the lowest *P*-value. We estimated the genome-wide q-value (FDR) for all 15,132 genes according to the Benjamini-Hochberg formulation, employing the R function p.adjust. We selected those genes and SNPs with q-value less than 0.1 for our final list of detected *cis*-eQTLs.

In order to check the distribution of SNP distance from either a RefSeq annotated transcription start site (TSS) or transcription end site (TES) of the associated gene for all SNPs that passed gene-wide correction without genome-wide correction, we tested all SNPs within 1Mb of TSS and TES and then used Bonferroni correction to obtain the gene-wide adjusted *P*-value. Those SNPs with gene-wide p-value <0.05 were collected and their distances from TSS and TES were calculated (Supplementary Table 17).

10. Supplementary References

51   O'Rahilly, R. & Müller, F. *The Embryonic Human Brain. An Atlas of Developmental Stages*. 3rd edn, (Wiley-Liss, 2006).

52   Judaš, M. in *Med Radiol Diagn Imaging* (ed D Prayer) 81-146 (Springer-Verlag, 2010).

53   Kostović, I. & Judaš, M. in *The Cognitive Neurosciences* (ed M.S. Gazzaniga) 29-47 (MIT Press, 2009).

54   Sidman, R. L. & Rakic, P. in *Histology and Histopathology of the Nervous System* (eds W. Haymaker & R.D. Adams) 3-145 (C.C. Thomas Publisher, 1982).

55   Poliakov, G. I. in *Cytoarchitectonics of the Human Cerebral Cortex* (eds S.A. Sarkisov, I.N. Filimonov, & N.S. Preobrazhenskaya) 33-91 (Medgiz, 1949).

56   Sidman, R. L. & Rakic, P. Neuronal migration, with special reference to developing human brain: a review. *Brain Res* **62**, 1-35, (1973).

57   Brodmann, K. *Vergleichende Lokalisationslehre der Grosshirnrinde in ihren Prinzipien dargestellt auf Grund des Zellenbaues*. (Johann Ambrosius Barth Verlag, 1909).

58   Irizarry, R. A., Ooi, S. L., Wu, Z. & Boeke, J. D. Use of mixture models in a microarray-based screening procedure for detecting differentially represented yeast mutants. *Stat Appl Genet Mol Biol* **2**, Article1, (2003).

59   Benovoy, D., Kwan, T. & Majewski, J. Effect of polymorphisms within probe-target sequences on olignonucleotide microarray experiments. *Nucleic Acids Res* **36**, 4417-4423, (2008).

60   Duan, S., Zhang, W., Bleibel, W. K., Cox, N. J. & Eileen Dolan, M. SNPinProbe_1.0: A database for filtering out probes in the Affymetrix GeneChip® Human Exon 1.0 ST array potentially affected by SNPs. *Bioinformation* **2**, 469-470, (2008).

61   Okoniewski, M. J. & Miller, C. J. Comprehensive analysis of Affymetrix exon arrays using BioConductor. *PLoS Comput Biol* **4**, 1-6, (2008).

62   Benjamini, Y. & Hochberg, Y. Controlling the False Discovery Rate: A Practical and Powerful Approach to Multiple Testing. *Journal of the Royal Statistical Society. Series B (Methodological)* **57**, 289-300, (1995).

63   Huang, D. W., Sherman, B. T. & Lempicki, R. A. Systematic and integrative analysis of large gene lists using DAVID bioinformatics resources. *Nat. Protocols* **4**, 44-57, (2008).

64   Huang, D. W., Sherman, B. T. & Lempicki, R. A. Bioinformatics enrichment tools: paths toward the comprehensive functional analysis of large gene lists. *Nucleic Acids Research* **37**, 1-13, (2009).

65   Langfelder, P. & Horvath, S. WGCNA: an R package for weighted correlation network analysis. *BMC Bioinformatics* **9**, 559, (2008).

66   Hu, Z. J., Hung, J. H., Wang, Y., Chang, Y. C., Huang, C. L., Huyck, M., & DeLisi, C. VisANT 3.5: multi-scale network visualization, analysis and inference based on the gene ontology. *Nucleic Acids Research* **37**, W115-W121, (2009).

67   Kumar, R. A. & Christian, S. L. Genetics of autism spectrum disorders. *Curr Neurol Neurosci Rep* **9**, 188-197, (2009).

68   Allen, N. C. *et al.* Systematic meta-analyses and field synopsis of genetic association studies in schizophrenia: the SzGene database. *Nat Genet* **40**, 827-834, (2008).

69   Fertuzinhos, S. *et al.* Selective depletion of molecularly defined cortical interneurons in human holoprosencephaly with severe striatal hypoplasia. *Cereb Cortex* **19**, 2196-2207, (2009).

70   Clancy, B. *et al.* Web-based method for translating neurodevelopment from laboratory species to humans. *Neuroinformatics* **5**, 79-94, (2007).

71   Paxinos, G., Halliday, G., Watson, C., Koutcherov, Y. & Wang, H. *Atlas of the Developing Mouse Brain* (Academic Press – Elsevier, 2007).

72   Schambra, U. *Prenatal Mouse Brain Atlas* (Springer, 2008).

73   Meyer, G. Genetic control of neuronal migrations in human cortical development. *Adv Anat Embryol Cell Biol* **189**, 1 p preceding 1, 1-111, (2007).

74   Campbell, D. B. *et al.* A genetic variant that disrupts MET transcription is associated with autism. *Proc Natl Acad Sci U S A* **103**, 16834-16839, (2006).

75   Südhof, T. C. Neuroligins and neurexins link synaptic function to cognitive disease. *Nature* **455**, 903-911, (2008).

76   Lawson-Yuen, A., Saldivar, J. S., Sommer, S. & Picker, J. Familial deletion within NLGN4 associated with autism and Tourette syndrome. *Eur J Hum Genet* **16**, 614-618, (2008).

77   Qi, H. B. *et al.* Positive association of neuroligin-4 gene with nonspecific mental retardation in the Qinba Mountains Region of China. *Psychiatr Genet* **19**, 1-5, (2009).

11. Supplementary Tables

Supplementary Tables are provided in a single Microsoft Excel file.

Supplementary Table 1. Donor/specimen metadata

This table summarizes donor information, including sex, age, ethnicity, pH, PMI, cause of death, and medical history for each human brain subject. Brain tissue was obtained from clinically normal donors and multiple brain specimens per period were analyzed to reduce the effects of individual variation. Demographic and quality control characteristics were as follows: age, 5.7 weeks postconception (PCW) to 82 years (Y); sex, 31 males and 26 females; PMI, 12.11±8.63 (mean±SD) hours; pH, 6.45±0.34 (mean±SD).

Supplementary Table 2. List of CNVs per specimen

Complete list of predicted copy number variations (CNVs) in each individual donor. Putative CNVs were predicted by two different algorithms (cnvPartition in GenomuStudio and PennCNV) using SNP intensity data generated by Illumina Human Omni 2.5-Quad Bead Chips. After validation of genomic normality, 57 brains were used in the transcriptome analysis.

Supplementary Table 3. Tissue sample metadata

This table summarizes quality control data for individual tissue samples, including RNA integrity number (RIN) and tissue dissection score (DS). Averaged RIN for each sample was 8.83±0.93 (mean±SD), and only those with a RIN above 5 and DS above 2 were processed for exon array analysis.

Supplementary Table 4. List of exon array CEL files

List of all exon array CEL files that passed the quality control steps throughout microarray cDNA preparation, hybridization, and outlier detection (Supplementary Information 5). A total of 1,340 samples were considered in downstream analyses.

Supplementary Table 5. List of region-enriched DEX genes

This table shows spatially DEX genes that were enriched in or restricted to only one of the regions (region-enriched genes). Using a combination of a sliding window algorithm and two-sample t-test, region-enriched DEX genes were analyzed within the periods of 3-7, 4-8, 5-9, 6-10, 7-11, 8-12, 9-13, 10-14, 11-15, respectively. The fold differences were calculated by comparing the gene expression value from one region of interest with another region that showed the second highest expression value. A gene with greater than 2-fold difference in a given window was considered to be region-enriched. The post hoc group assignment analysis was performed by calculating the fold differences attributed to the two periods bordering each side of the developmental groups (6-7 and 8-9 for prenatal-postnatal group; 11-12 and 13-14 for postnatal adult group). If the fold difference was greater than 1.5, the gene was assigned to that developmental group, resulting in either one or both group(s) being assigned.

Supplementary Table 6. Tukey's pairwise analysis of human and mouse *ANKRD32* isoforms

The Tukey's pairwise comparison was performed after ANOVA to determine which pairs of NCX areas were significantly different from each other. The TukeyHSD function in R was used to calculate the gene expression mean difference and corresponding *P*-value.

Supplementary Table 7. List of sex-biased DEX genes

Differentially expressed genes between males and females were analyzed by a combination of a sliding window algorithm and t-test. The window size was set as 5 in order to ensure adequate representation of both sexes, and periods 2-6, 3-7, 4-8, 5-9, 6-10, 7-11, 8-12, 9-13, 10-14, 11-15 were examined. For each window, a two-sample t-test was applied to determine sex-biased genes in the same region (cutoff of FDR 0.01 and 2-fold difference). The post-hoc group assignment analysis was performed by calculating the fold differences attributed to the two periods bordering each side of the developmental groups (6-7 and 8-9 for prenatal-postnatal group; 11-12 and 13-14 for postnatal-adult

group). If the fold difference was greater than 1.5, the gene was assigned to that developmental group, resulting in either one or both group(s) being assigned the gene.

Supplementary Table 8. List of sex-biased DEU genes
Genes with differential exon usage between males and females were analyzed by a combination of splicing index and two-sample t-test under a sliding window algorithm. The window size was set as 5 in order to ensure adequate representation of both sexes, and periods 2-6, 3-7, 4-8, 5-9, 6-10, 7-11, 8-12, 9-13, 10-14, 11-15 were examined. For each window, exon cluster expression was normalized by dividing its gene-level expression. The splicing index was then calculated as a "fold change" between the normalized levels of each exon cluster to determine the sex-specific DEU (cutoff of FDR <0.01 and 2-fold difference).

Supplementary Table 9. Co-expression network modules
List of 29 modules corresponding to spatio-temporal patterns identified by weighted gene co-expression network analysis (WGCNA) with its functional interpretation, list of hub genes, and result of gene ontology analysis performed by DAVID algorithm. Top 10 hub genes are listed for each module, though some consist of less than 10 due to small module sizes. Two large modules (M20; 3,287 genes and M2; 2,745 genes) appeared to be simultaneously co-regulated across all regions with opposite developmental trajectories (Supplementary Figs 21 and 22). In addition to the predominant temporal patterns, region-specific modules were also identified, such as M9 (MD), M19 (CBC), M23 (STR). Several modules exhibited no obvious spatio-temporal expression patterns but were enriched in genes associated with cell cycle (M1), cytoskeleton (M3), olfactory receptors (M13), and sex-specific transcription (M22).

Supplementary Table 10. Correlation between network modules and neurobiological categories
The correlation coefficient was calculated between each network module and functional gene group of specific neurobiological categories. Manually generated annotations for various functional groups and consisting gene list are also provided in Supplementary Table 12. The first principle component of each module expression (eigengene by WGCNA analysis) and each gene group were applied for correlation coefficient computation. Notably, M8 module (high in prenatal NCX, HIP, and AMY) showed strong correlation with layer 2 to 6 cortical glutamatergic neurons, while M15 module (high in postnatal NCX, HIP, AMY, and STR) showed strong correlation with dendrite development, synapse development, glial cells (astrocytes, myelination, and oligodendrocytes), GABA shift, and certain cortical GABA cell types. Also, M20 module (high in prenatal) showed strong correlation with cell proliferation, neuron differentiation, neuron migration, and cortical deep layer glutamatergic neurons, while it shows strong anti-correlation with synapse development, dendrite development, glial cells (astrocytes, microglia, oligodendrocytes, and myelination), GABA shift, and certain cortical GABA cell types. On the contrary, correlation of M2 module (high in postnatal) showed opposite trend with these functional groups.

Supplementary Table 11. Correlation between network modules and confounders
This table shows correlation between network modules and all the factors associated with the samples, including possible confounders (RIN, PMI, pH, and DS). To check the effects of RIN, PMI, pH, and dissection on module identification, the coefficient of determination (r^2) and P-value was calculated after constructing a linear ANOVA model. The modules with r^2 of any factor greater than 0.1 and r^2 of any confounder (RIN, PMI, pH, and DS) larger than the largest r^2 of the main factors (age, region and sex) were considered as modules corresponding to confounders. Five modules were detected as confounder-related modules and removed from further analyses. One module (grey), consisting of genes not assigned to any other module, was also removed.

Supplementary Table 12. Gene lists for neurobiological categories
List of the manually generated gene group annotations for various neurobiological categories. We summarized the gene list into three major categories: neurodevelopmental processes, neural cell types, and major neurotransmitter systems. Each category was classified into functional groups and subgroups based on existing GO categories (www.geneontology.org) and published data from model organisms and human medical genetics.

Supplementary Table 13. Genes correlated with genes involved in neurodevelopmental processes

The correlation coefficient was calculated between each functional gene group involved in specific neurodevelopmental processes and all genes expressed. The first principle component of each gene group was computed against each gene expression level. Top 100 genes are listed.

Supplementary Table 14. Genes correlated with genes expressed in specific neural cell types
The correlation coefficient was calculated between each functional gene group involved in specific neural cell types and all genes expressed. The first principle component of each gene group was computed against each gene expression level. Top 100 genes are listed.

Supplementary Table 15. Transcripts correlated with ASD-associated genes
This table shows the top 50 correlated transcripts with autism spectrum disorder (ASD) related genes, which were compiled from recent reviews and relevant databases (Supplementary information 6.10). Correlation coefficient (r^2) was calculated between the expression level of each gene and all transcripts expressed. Functional annotation suggested that these genes were predominantly associated with phosphoprotein (Bonferroni-adjusted P=1.3 × 10^{-30}), synapse (Bonferroni-adjusted P=9.1 × 10^{-30}), synaptic transmission (Bonferroni-adjusted P=5.8× 10^{-26}), cell junction (Bonferroni-adjusted P=1.5 × 10^{-20}), neuron projection (Bonferroni-adjusted P=3.4 × 10^{-19}), and ionic channels (Bonferroni-adjusted P=3.8 × 10^{-17}).
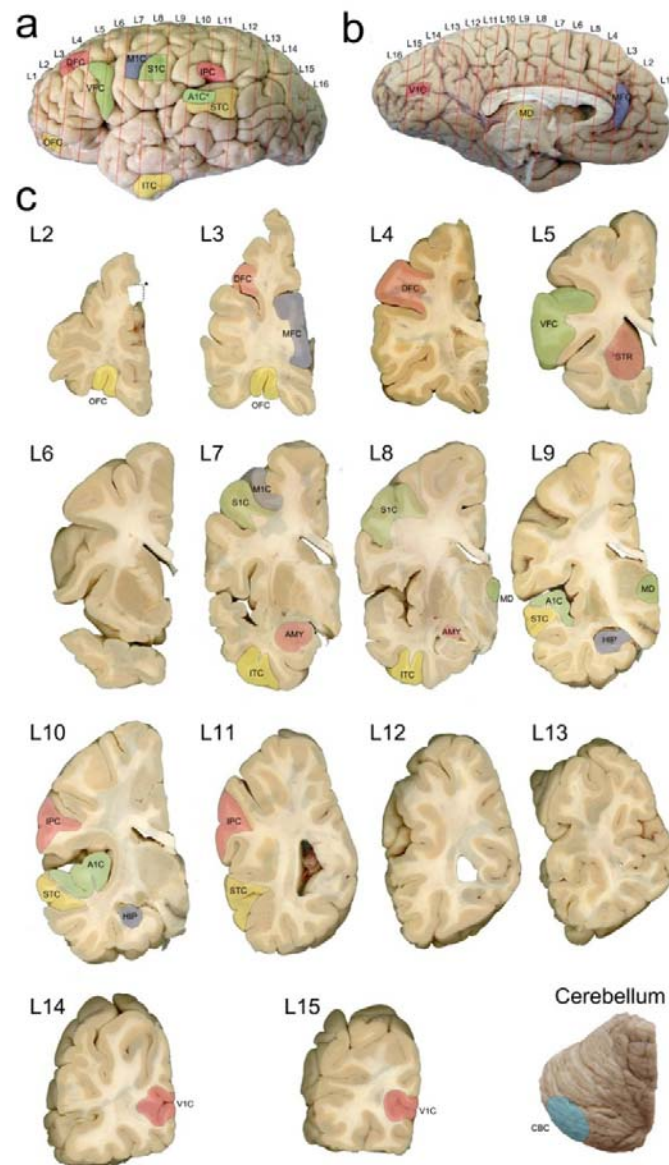
Supplementary Table 16. Transcripts correlated with schizophrenia-associated genes
This table shows the top 50 correlated transcripts with schizophrenia related genes, which were compiled from recent meta-analyses and relevant databases (Supplementary information 6.10). Correlation coefficient (r^2) was calculated between expression level of each gene and all transcripts expressed. Functional annotation suggested that these genes were mainly associated with glycoprotein (Bonferroni-adjusted P=1.5 × 10^{-16}), plasma membrane (Bonferroni-adjusted P = 1.5 × 10^{-12}), ionic channel (Bonferroni-adjusted P=2.6 × 10^{-9}), synaptic transmission (Bonferroni-adjusted P=3.8 × 10^{-7}), and phosophoprotein (Bonferroni-adjusted P=5.3 × 10^{-7}).
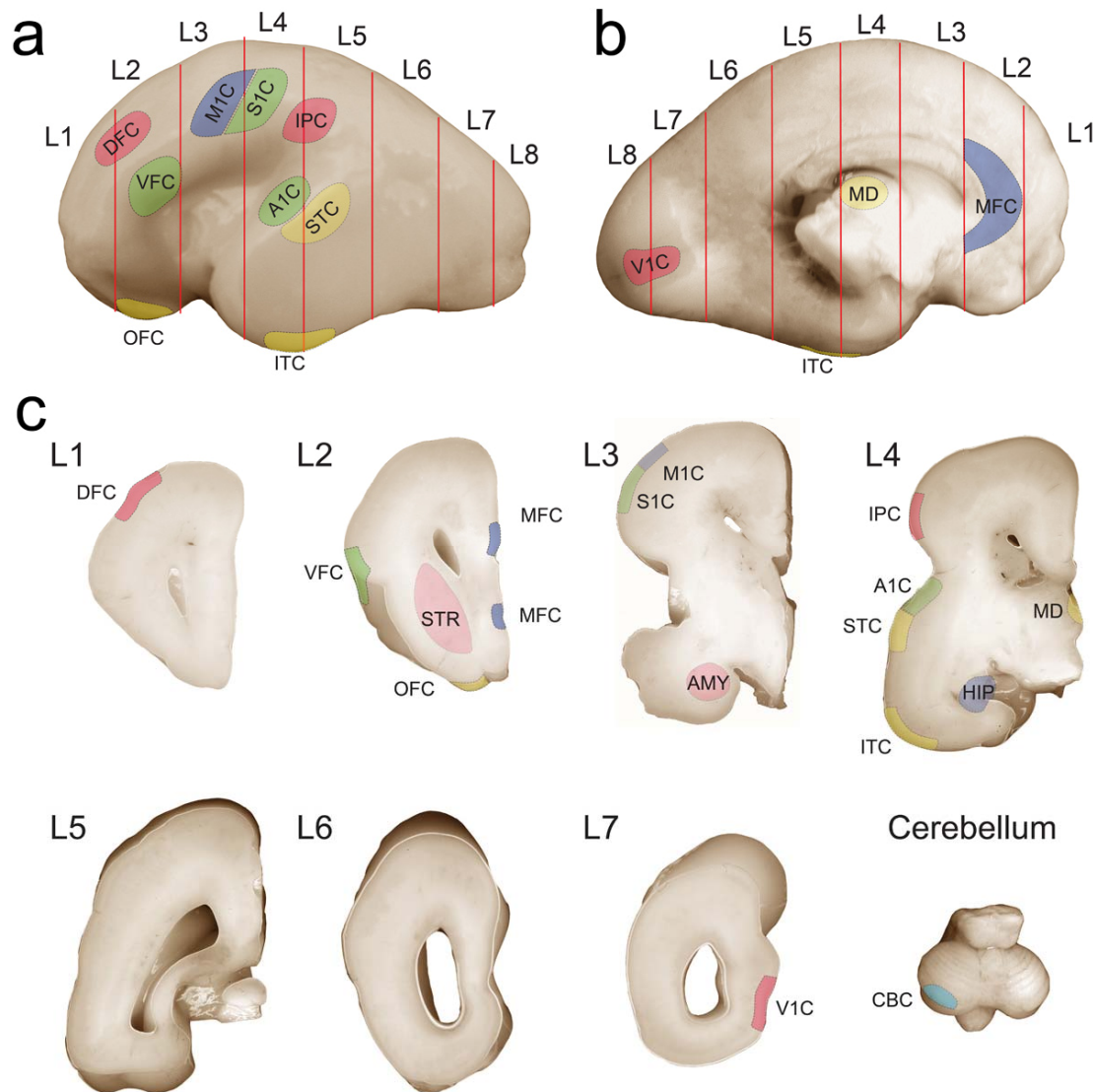
Supplementary Table 17. Regional *cis*-eQTLs
This table shows *cis*-eQTL within 10kb flanking two ends of the target gene, detected in 6 brain regions (NCX, HIP, AMY, STR, MD and CBC). Rows in red are eQTLs with genome-wide FDR <0.1, rows in black are eQTLs with genome-wide FDR <0.2. SNP count is the number of local SNPs tested for the gene. MAF is minor allele frequency in our dataset. HWE p-value is the Hardy-Weinberg-Equilibrium test p-value of our genotyping result. Number of BB calls is the number of individuals with genotype of homozygous minor allele. WALD *P*-value is the original association p-value calculated by PLINK. Covariants *P*-value is the WALD p-value with co-factors of RIN, PMI, sex, ethnicity, and first two principle components. Gene-wide *P*-value was calculated from the original WALD *P*-value after Bonferroni correction by number of local SNPs. Permutation *P*-value was calculated from label-swapping adaptive permutation by PLINK with maximum of 1,000,000 times. FDR *P*-value was calculated from the Gene-wide *P*-value after genome-wide FDR correction.
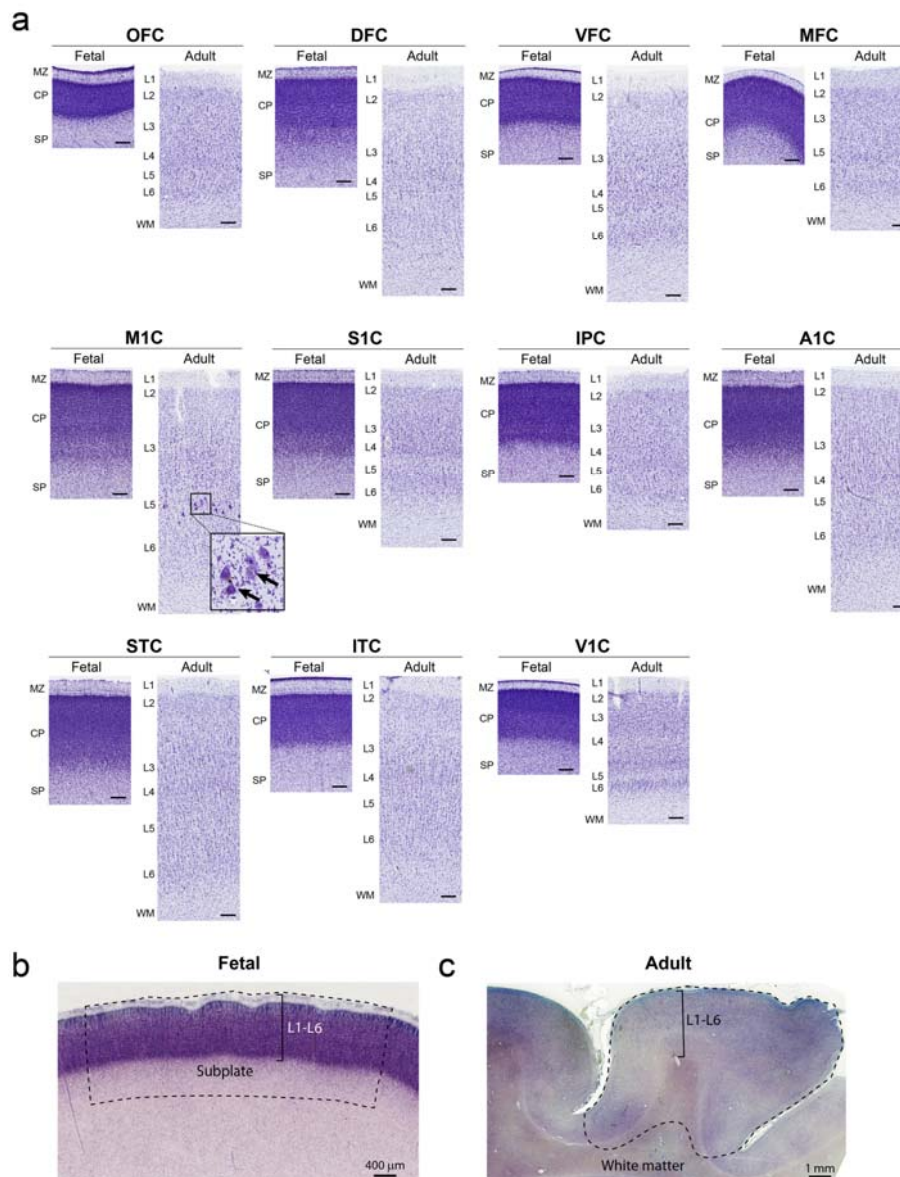
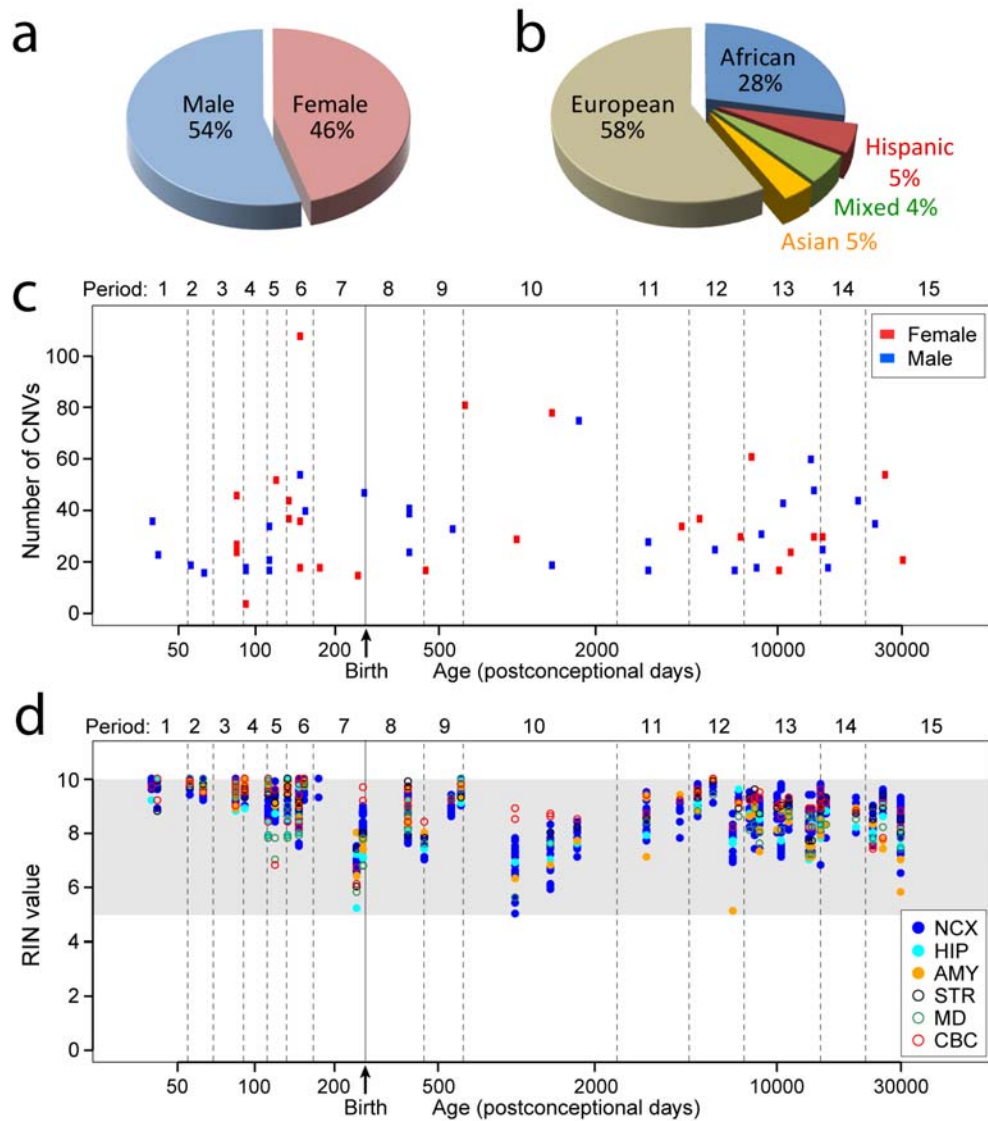## 12. Supplementary Figures

Supplementary Figure 1 | Demarcation of adult brain regions and NCX areas. a-c, Representative adult human brain images from period 14 are shown illustrating the sampling locations depicted on the lateral (a) and medial (b) surfaces of the hemisphere and the dorsal surface of the cerebellar hemisphere (c). Relative sizes of the sampled regions of interest are depicted on coronal slices (c, L2 – L15) of the left cerebral hemisphere. Red lines in (a) and (b) represent locations of coronal sections. The posterior side of the slice is shown, and the average section thickness is 1 cm. Brain regions and NCX areas of interest are represented by different colors and two or three letter abbreviations (for full names see section 2.2 of the Supplementary Information). A1C* is located on the temporal bank of the lateral sulcus (i.e., planum temporale and transverse gyrus of Heschl), and cannot be observed on the lateral view of the hemisphere; for illustrative purposes only, relative size and position of the A1C* was depicted on the lateral surface. The dotted line and asterisk (L2) depict an artifact during tissue processing. For detailed sampling procedures see section 2.2 of the accompanying Supplementary Information. These images were generated using fixed brain specimens not used to generate transcriptome data.
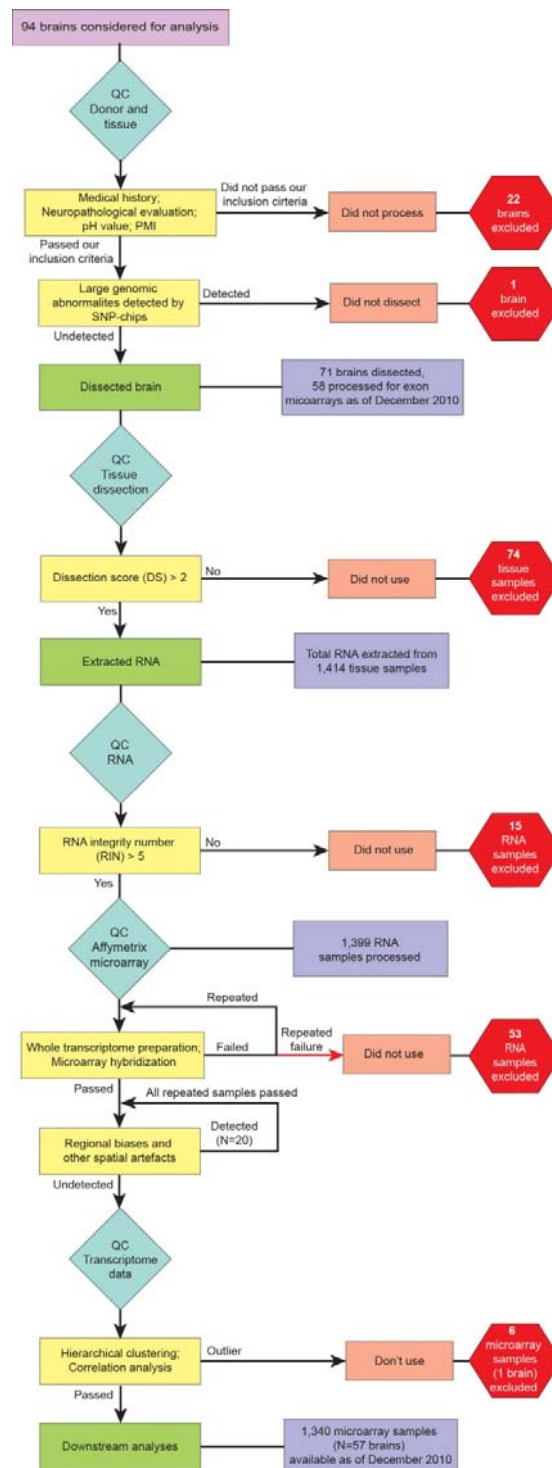
Supplementary Figure 2 | Demarcation of fetal brain regions and NCX areas. a-c, Representative fetal human brain images from period 6 are shown illustrating the sampling locations of tissues used for transcriptome analysis. Relative positions of the regions of interest are depicted on the lateral (a) and medial (b) surfaces of the hemisphere and the dorsal surface of the cerebellar hemisphere (c). Relative sizes of the sampled regions of interest are depicted on coronal slices (c, L1 – L7) of the left cerebral hemisphere. Red lines in (a) and (b) represent locations of coronal sections. The posterior side of the slice is shown, and the average section thickness is 0.5 cm. Regions of interest are represented by different colors and two or three letter abbreviations (for full names see section 2.2 of the Supplementary Information). In total, 16 regions of interest were sampled as follows: 5 regions from the frontal lobe cortex (OFC, DFC, VFC, MFC and M1C), 2 regions from the parietal lobe cortex (S1C and IPC), 4 regions from the temporal lobe cortex (A1C, STC, ITC and HIP), 1 region from the occipital lobe cortex (V1C), 3 regions from subcortical structures (MD, AMY and STR) and 1 region from the cerebellum (CBC). Sampled regions of interest always contained cortical plate and part of the underlying subplate zone. For detailed sampling procedures see section 2.2 of the Supplementary Information. These images were generated using fixed brain specimens not used to generate transcriptome data.
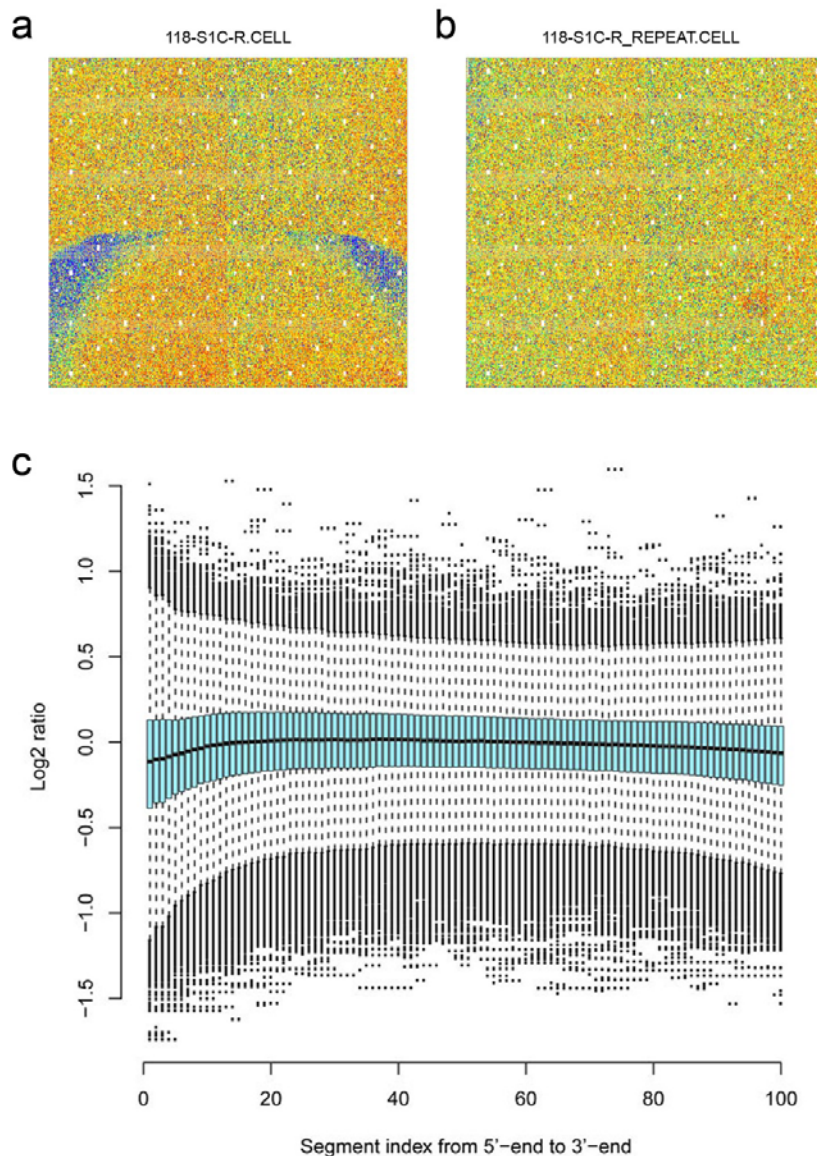
Supplementary Figure 3 | Histological evaluation and dissection of NCX areas. a, Nissl staining was used to validate the following NCX areas: OFC, DFC, VFC, MFC, M1C, S1C, IPC, A1C, STC, ITC, and V1C. Sampling from fetal (period 6) and adult (period 14) specimens was carried out according to the methods and criteria used for the dissection of exon array samples. Staining in fetal NCX areas revealed densely packed neurons in the cortical plate (CP) with no obvious distinctions among cortical layers. The marginal zone (MZ) and subplate (SP) were present in the fetal samples. Conversely, adult NCX neurons were at a lower density and were arranged in layers (L1–L6) containing neurons of distinct size and shape (e.g., L5-specific Betz cells in M1C; arrow). The adult cortical layers had a greater thickness than the fetal cortical plate, and white matter (WM) was apparent below the laminar pattern. Scale bars, 250 μm. **b, c,** Nissl staining images of the fetal (b, period 6) and adult (c, period 14) VFC are shown to illustrate the microscopic boundaries of the NCX tissue sampled for transcriptome analysis. In the fetal brains (b), the entire cortical plate (L1–L6) and adjacent subplate zone was sampled. In the adult brains (c) all six cortical layers (L1–L6) and underlying gyral white matter were sampled. Dotted lines in (b) and (c) represent dissection boundaries. These three images were generated using fixed brain specimens not used for the exon array analysis.
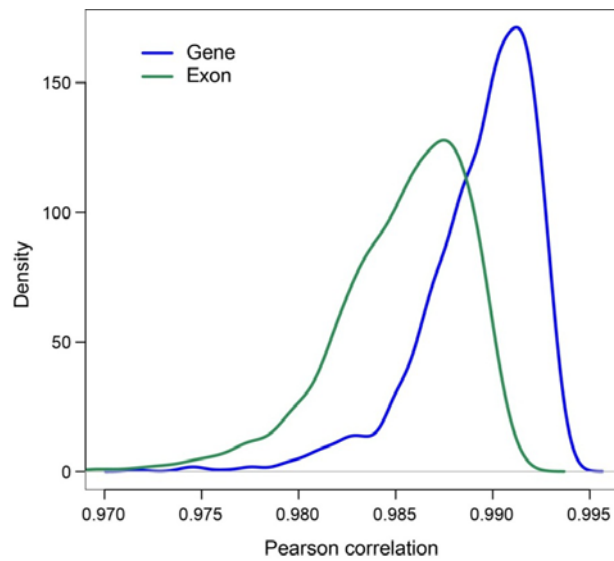
Supplmentary Figure 4 | Demographics, genotyping, and RNA integrity of analyzed brain specimens. **a**, Sex distribution of specimens. **b**, Ethnicity distribution of specimens according to SNP genotypes. **c**, Number of CNVs per individual specimen distributed across sexes and time periods. **d**, RNA quality was evaluated by determining the RNA integrity number (RIN) for each sample (8.83 ± 0.93, mean$\pm$SD), and only those with a RIN ≥5 were processed (1,340 samples). Age is represented as $\log_2$–transformation of days postconception. Time of birth, separating prenatal from postnatal periods, is marked by vertical solid line.
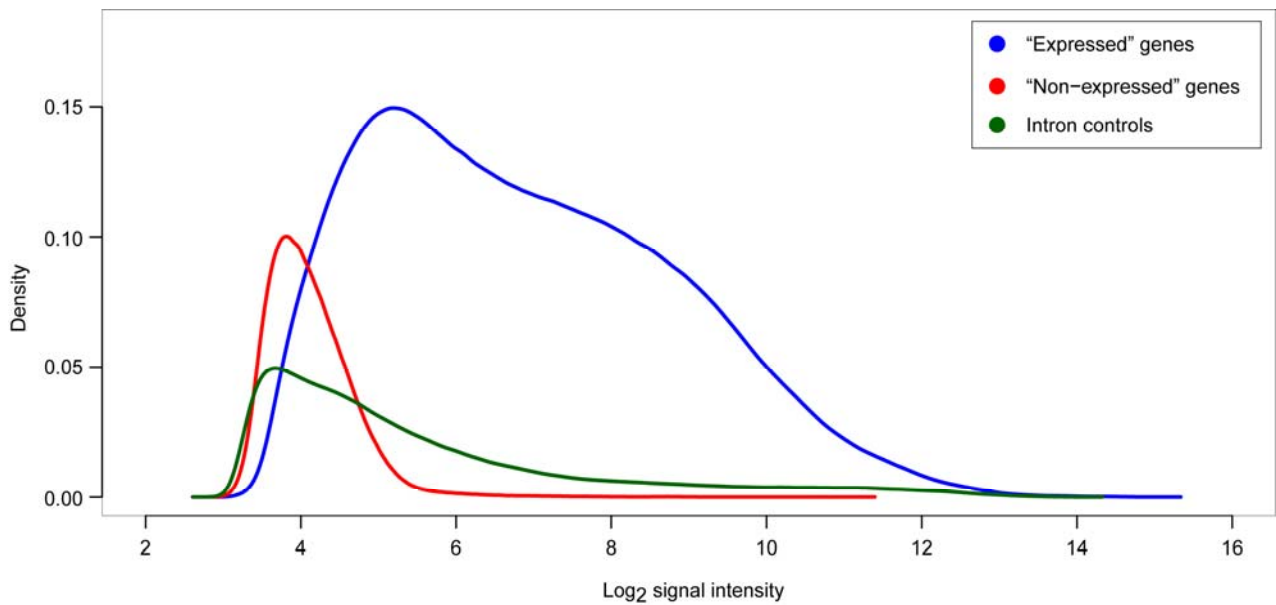
Supplementary Figure 5 | Quality control workflow. Blue diamonds represent a quality control (QC) step, yellow squares represent criteria used to determine quality of the samples, green squares represent actions taken after quality control, red hexagons represent samples excluded from further analysis, and purple squares represent samples considered for further analysis. For details see Supplementary Information 2.3.
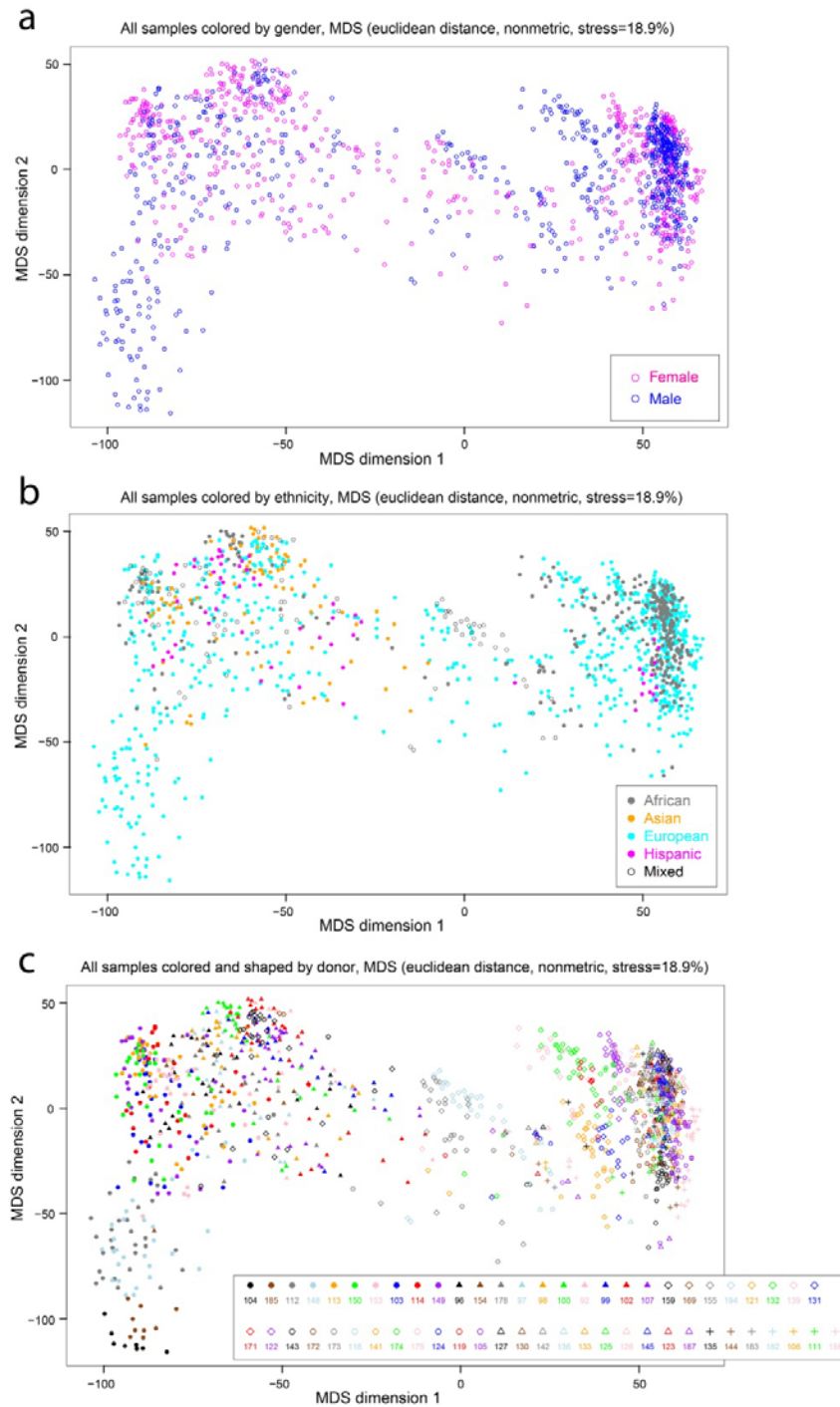
Supplementary Figure 6 | Exon array hybridization quality control. a, b, The color of each dot in the plot represents relative intensity of a probe in the target chip compared to the average intensity of that probe in the same batch of chips. Individual probes of one gene were randomly located on the whole chip, and consequently there should be no obvious spatial pattern in the plot. The relative intensity plot of a low quality chip for sample 118-S1C-R with spatial artifacts (a) and the relative intensity plot of the high quality replicate chip for the same sample (118-S1C-R_REPEAT), without any obvious spatial artifact (b). **c,** The longest transcript of each gene was split into 100 segments with equal length, from 5'-end to 3'-end, and the log2-transformed signal intensity ratio for each segment was calculated compared with the expression of the whole gene across 1,340 chips. The statistics of the ratios for all genes were displayed by a box plot for each segment. The flat solid line consisting of the mean lines of the box plots displays the array hybridization uniformity.
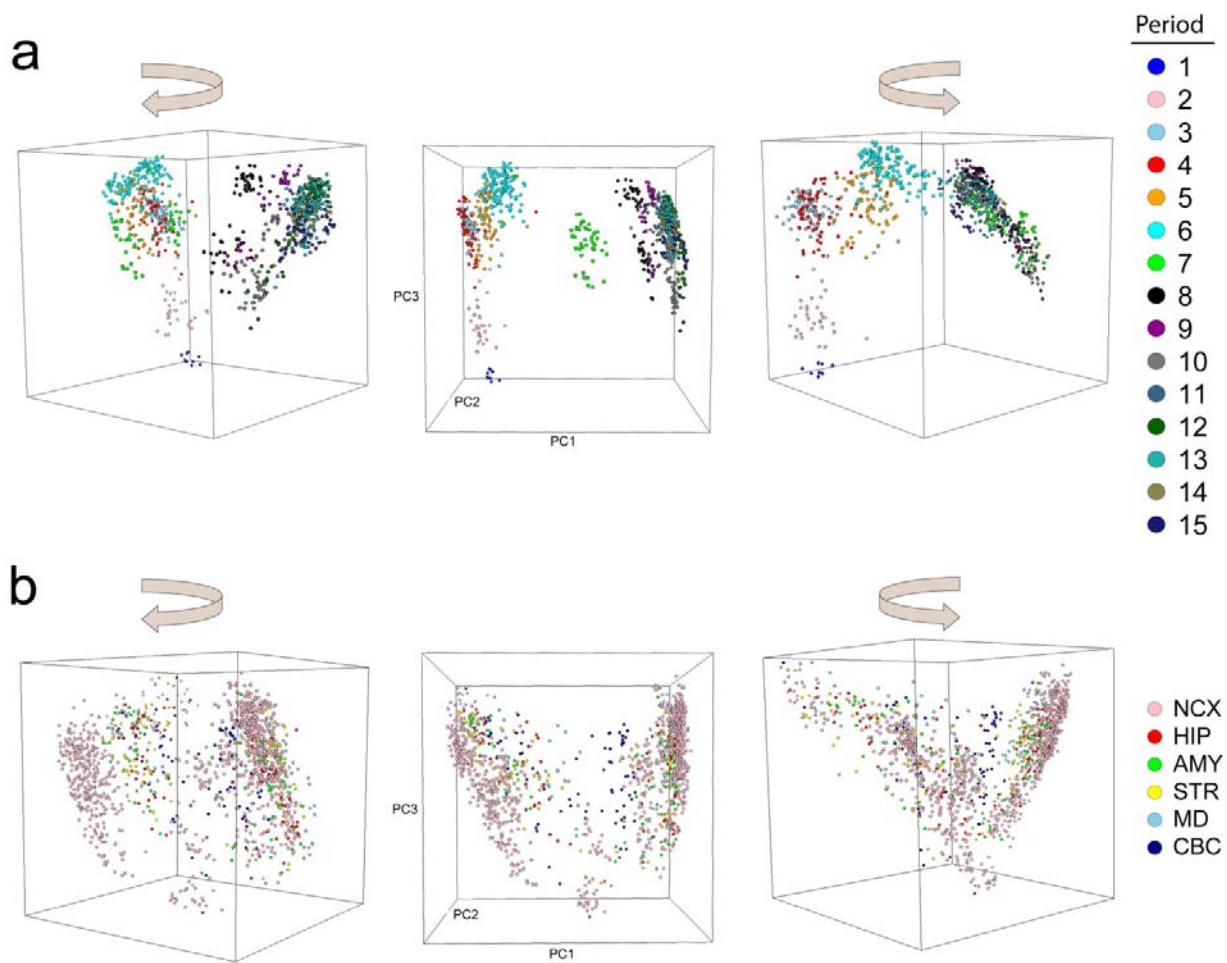
Supplementary Figure 7 | Expression analysis with and without SNP-containing probe sets. The gene and exon (probe set)-level expression analyses were evaluated twice, including and excluding 105,271 probes with SNPs. The Pearson correlation analysis was performed to show the degree to which SNPs affect the expression data. The density plots give the distribution of Pearson Correlation Coefficient (PCC) values for all 1,340 samples (gene and exons are represented by blue and green lines, respectively). The majority of PCC values (98.8%) were within the range of 0.980-0.995 for gene and of 0.975-0.995 for exon, suggesting that SNPs have a minimal effect on gene and exon expression.
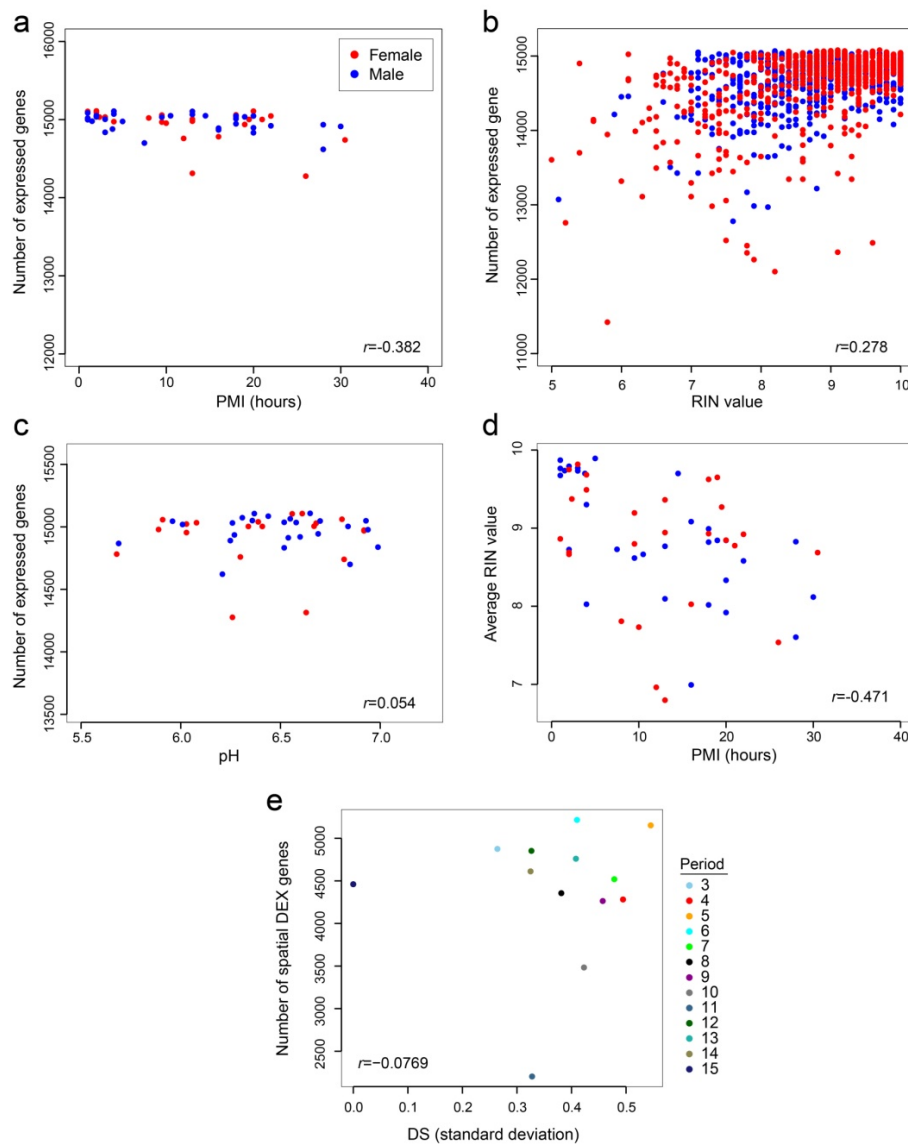
Supplementary Figure 8 | Hierarchical clustering of NCX samples. Dendrogram branching shows hierarchical sample clustering of NCX. The colors underneath label the potential confounders: age (blue to red representing younger to old), sex (light blue, male; pink, female), ethnicity (African, blue; African/European, green; Asian, yellow; European, light brown; Hispanic, dark red), PMI (low to high representing blue to red), dissection score (low to high representing blue to red), RIN (low to high representing blue to red), and the array processing site (Site 1, blue; Site 2, white). The samples clustered predominately by age (periods) and not by sex, ethnicity, PMI, dissection score, RIN, or the array processing site. Three major clusters (a stage 1 and 2 cluster, a prenatal cluster, and a postnatal cluster) were found in the NCX. Clustering data for other regional samples (HIP, AMY, STR, MD and CBC) are not shown but revealed the same trend.

Supplementary Figure 9 | Distribution plot of exon array signal intensities for "expressed", "non-expressed", and intronic controls. The "expressed" genes are defined by two criteria of $\log_2$-transformed signal intensity and DABG p-value (Supplementary information 6.1). The first group of genes included genes with averaged DABG P <0.01 in at least one region and log2 intensity ≥6 in at least one sample. These genes were considered as "expressed" genes (blue). The second group included genes whose averaged DABG P >0.01 or $\log_2$ intensity <6 in all samples and were considered "non-expressed" group (red). The final group is intronic controls (dark green) consisting of probe sets designed from intron regions of a set of housekeeping genes. Note the distinct distribution of "expressed" genes compared to "non-expressed" genes and intronic controls.

Supplementary Figure 10 | Multi-dimensional scaling according to sex, ethnicity, and donor. Two-dimensional multi-dimensional scaling plot showing genome-wide transcriptional similarity between any two samples. Each sample is represented as a single point. Proximity indicates transcriptional similarity between two samples. Euclidean distance of $\log_2$-transformed signal intensity (expression) values was used to measure the pairwise dissimilarity. The isoMDS function in the R package was used to create the configuration of all points in the two dimensional space. **a,** colors indicate sex. **b,** colors indicate ethnicity. **c,** colors and shapes indicate donor.

Supplementary Figure 11 | Principal component analysis. a, Three-dimensional plot of PCA of NCX samples across 15 time periods. Each point represents one NCX sample. Samples are colored by period. Three dimensional figures are rotated to provide a better view of the separation within prenatal (left) and postnatal (right) periods. **b**, PCA plot for all 1,340 samples across 6 brain regions and all time periods. Each point represents one sample. Samples are colored by brain region.
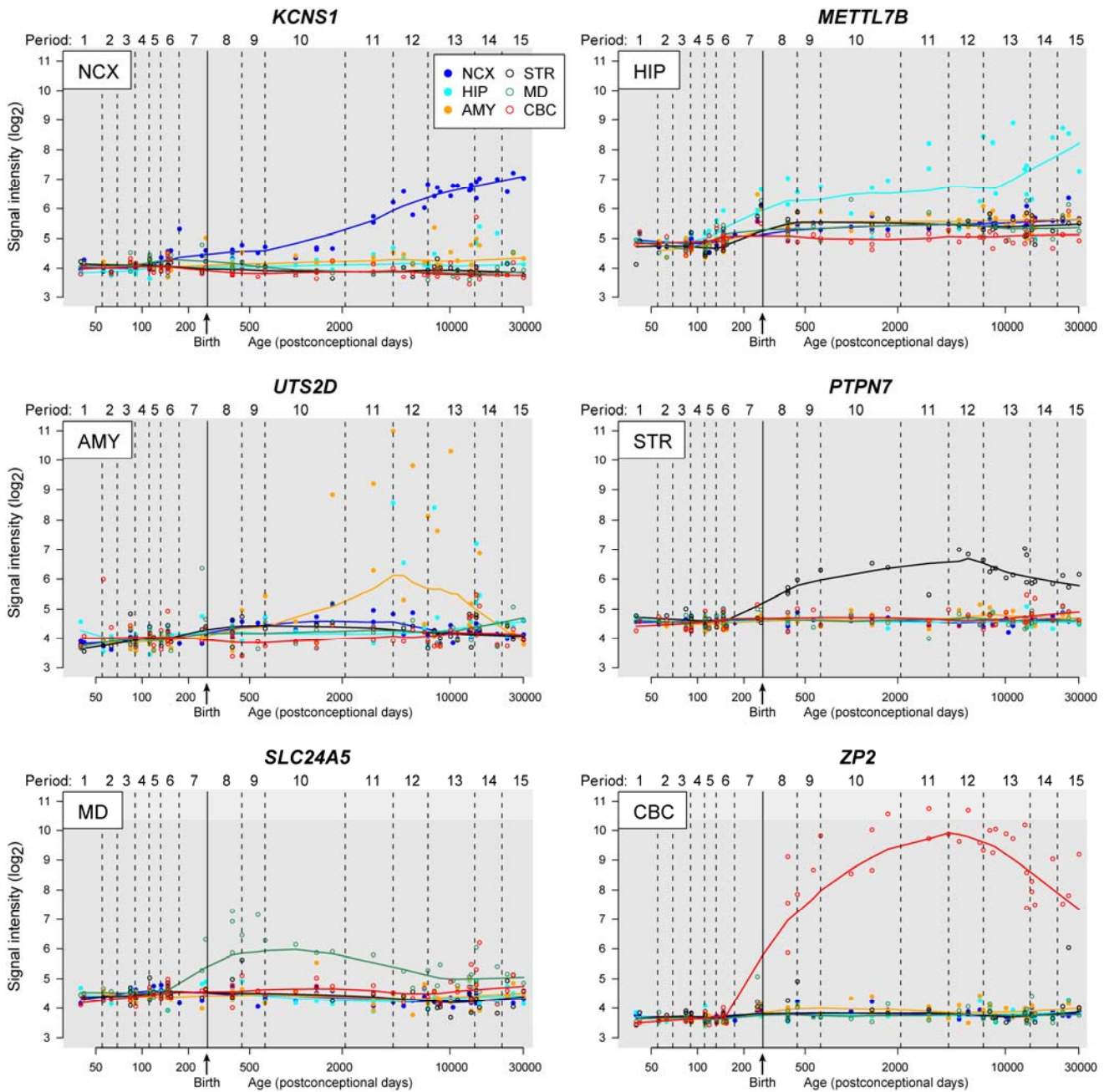
Supplementary Figure 12 | Correlations between PMI, pH, RIN, DS, and gene expression. a - c, Correlation of the number of expressed genes with PMI (a), RIN (b), and pH (c). Each data point represents one brain (a, c) or one sample (b). Weak anticorrelations and correlations were observed with PMI (Spearman correlation, *r*=-0.382) and RIN (Spearman correlation, *r*=0.278), respectively. No correlation was observed with pH (Spearman correlation, *r*=0.054). **d,** Correlation between PMI and RIN. Each data point represents one brain specimen. Y-axis is the averaged RIN of individual brain specimens. X-axis is PMI of the same specimens. The Spearman correlation is -0.471, indicating that PMI and RIN are anticorrelated. **e,** The Y-axis is the number of spatial DEX genes with significantly differential expression between brain regions and NCX areas detected by ANOVA test (FDR <0.01 and 2-fold difference) for the indicated period. The X-axis is the standard deviation of DS of all samples in that period. No significant correlation was observed between variation of DS and number of spatially DEX genes (Spearman correlation, *r* = -0.077). We limited this analysis to periods 3-15, when regions/areas of interest are well-defined using equivalent criteria and can be consistently followed across time, thus allowing us to assess whether the impact of variation in DS within the same stage contribute to differences in the number of detected spatially DEX genes for that particular period.
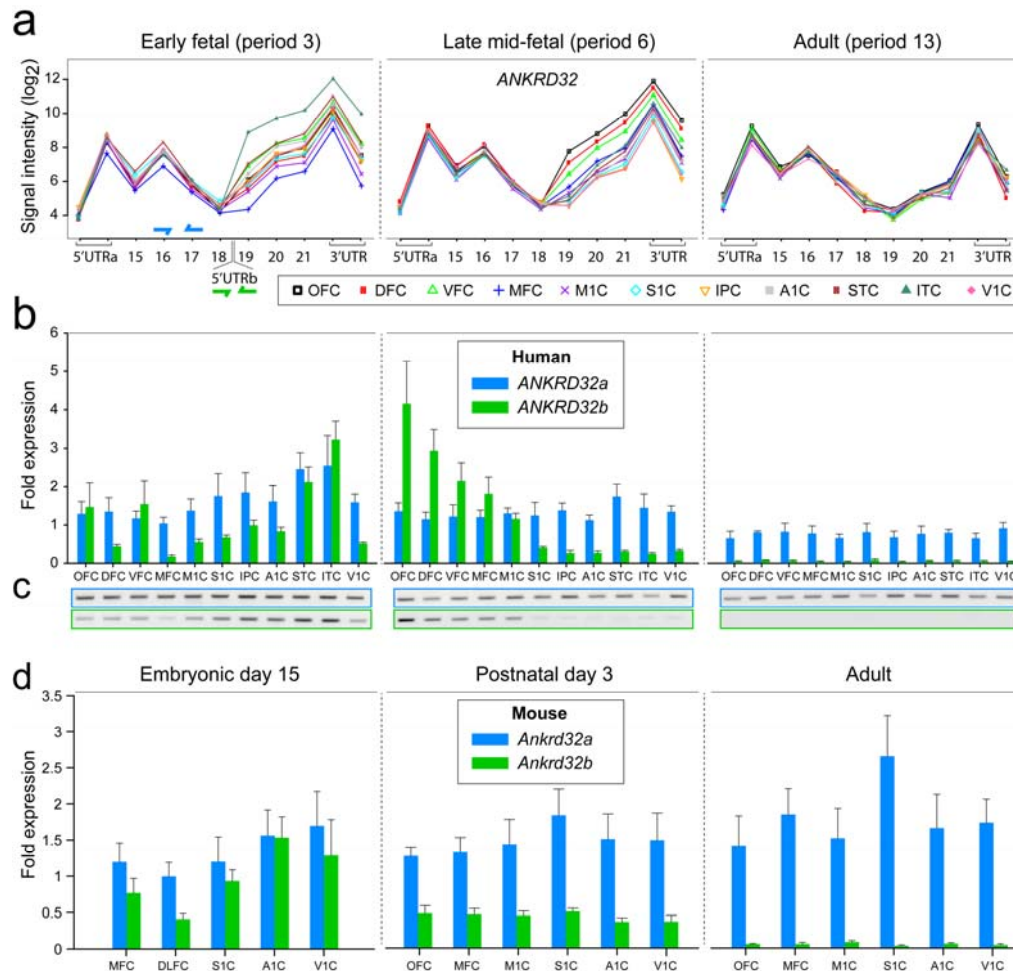
Supplementary Figure 13 | Five-fold jackknife procedure. The robustness of our DEX and DEU analysis models were tested randomly dividing samples into 5 groups and re-analyzing spatial/temporal DEX and DEU 5 times while leaving out one group of samples in each cycle. Overlap plots for DEX and DEU genes between whole dataset and each cycle are shown. The average overlap rates were as follows: spatial DEX (93.47%), temporal DEX (98.0%), spatial DEU (94.3%), and temporal DEU (99.4%). This analysis indicates that our findings did not depend on any particular sample.
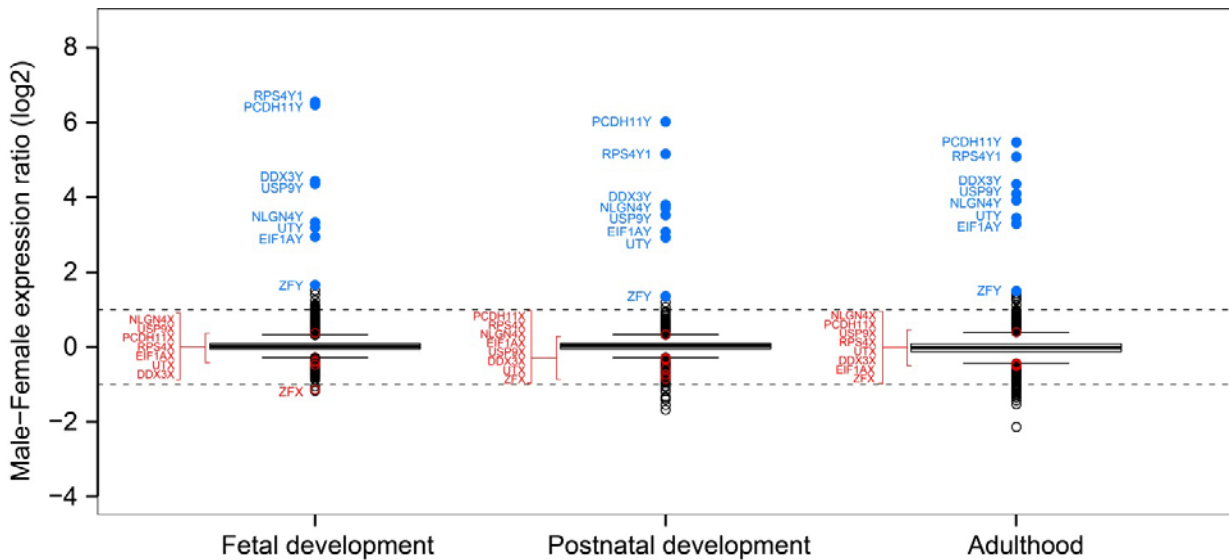
Supplementary Figure 14 | Prenatal region-enriched gene expression. An example of a transiently expressed and region enriched DEX gene for each region is shown. These genes were highly expressed during prenatal and in some cases early postnatal development in predominantly one region and then were not expressed or had low expression level in other regions. Samples and associated signal intensity values are colored by region.
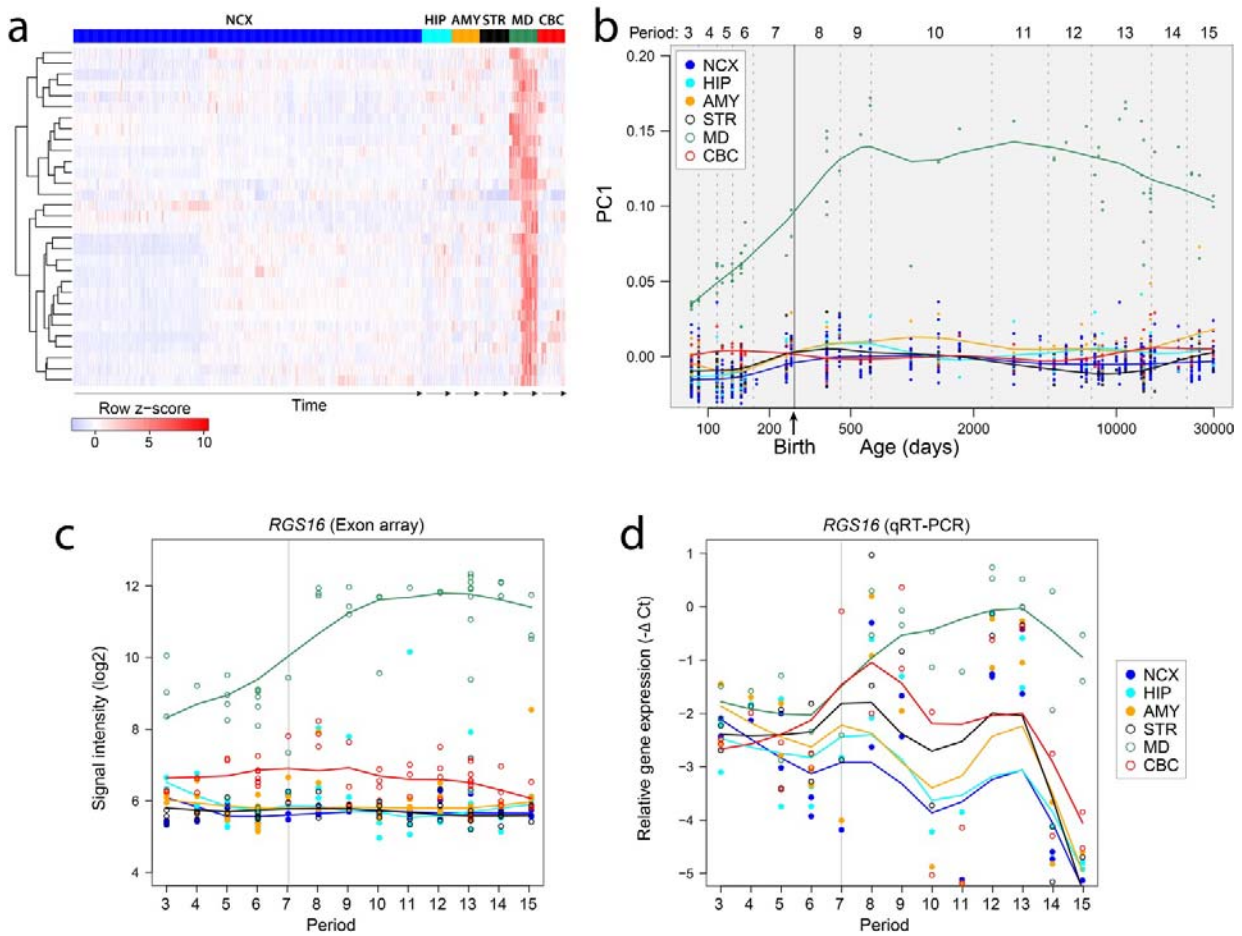
Supplementary Figure 15 | Postnatal region-enriched gene expression. An example of a transiently expressed and region enriched DEX gene for each region is shown. These genes were highly expressed during postnatal life in predominantly one region and then were not expressed or had low expression level in other regions. Samples and associated signal intensity values are colored by region.
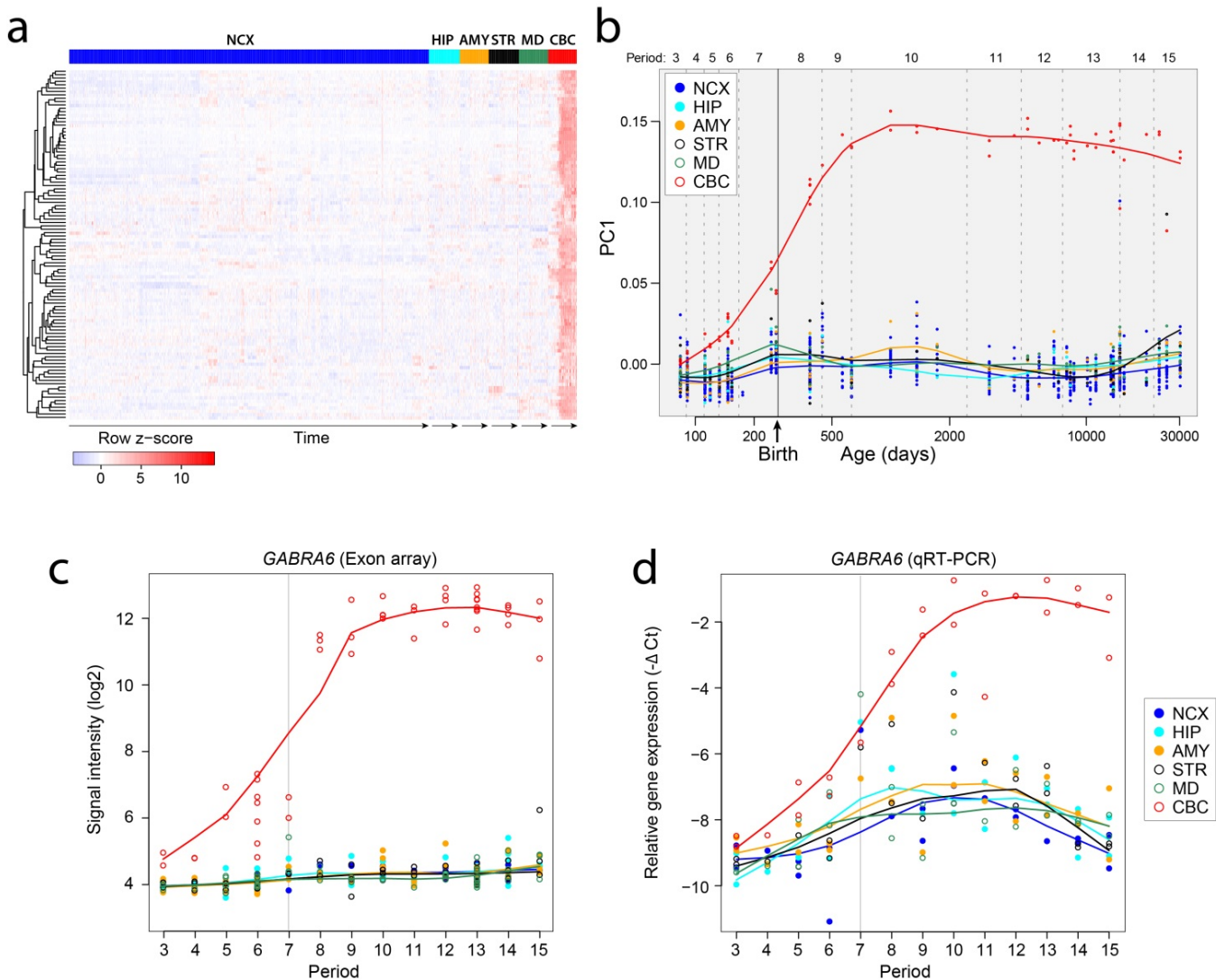
Supplementary Figure 16 | Spatio-temporal analysis of differential exon usage of *ANKRD32*. **a,** Plotted are log₂-transformed signal intensity levels (y-axis) for each probe set and the corresponding exons (x-axis) of *ANKRD32*. The exons are labeled according to RefSeq notation. The location of isoform specific primers used in b and c are depicted by blue (*ANKRD32a*) and green (*ANKRD32b*) arrows. **b,c,** qRT-PCR (**b**, mean ± SEM) and semi-quantitative RT-PCR (**c**) validation analyses of the long (blue) and short (green) *ANKRD32* isoforms (*ANKRD32a* and *ANKRD32b*, respectively) represented as relative gene expression levels. *ANKRD32a* was consistently expressed across early fetal (period 3), late midfetal (period 6), and adult NCX areas. In contrast, *ANKRD32b* exhibited significant differences in expression between areas of the early fetal and midfetal NCX (one-way ANOVA, $P=1.3\times10^{-5}$ and $P=1.9\times10^{-7}$, respectively; followed by Tukey's pairwise test; see Supplementary Table 6). During early fetal period 3, *ANKRD32b* was most highly enriched in the ITC and, to a lesser extent, in the STC (one-way ANOVA $P=1.3\times10^{-5}$, followed by Tukey's pairwise test). **d,** qRT-PCR in orthologous areas of the mouse NCX at equivalent developmental periods (see Supplementary Information 8) Primers were generated against the mouse genomic region orthologous to the human A*NKRD32b* 5'UTR. *Ankrd32a* and *Ankrd32b* isoforms were expressed as early as E15, which equates to approximately 12–13 PCW (period 3) in humans. *Ankrd32b* was expressed at lower levels compared to the *Ankrd32a* and was enriched in the prospective S1C, A1C, and V1C (see Supplementary Information 8 for tissue sampling) but not in the frontal cortex (one-way ANOVA, $P=9.2\times10^{-4}$, followed by Tukey's pairwise test). At P3, which approximately corresponds to 20 PCW (period 6) in humans, mouse *Ankrd32b* was expressed at low levels uniformly across NCX and was not enriched in any of the NCX areas, including the multiple frontal areas (one-way ANOVA, $P=0.14$). We detected substantial levels of the *Ankrd32a* but not the *Ankrd32b* in the adult mouse NCX, which was similar to what was observed in the adult human NCX.
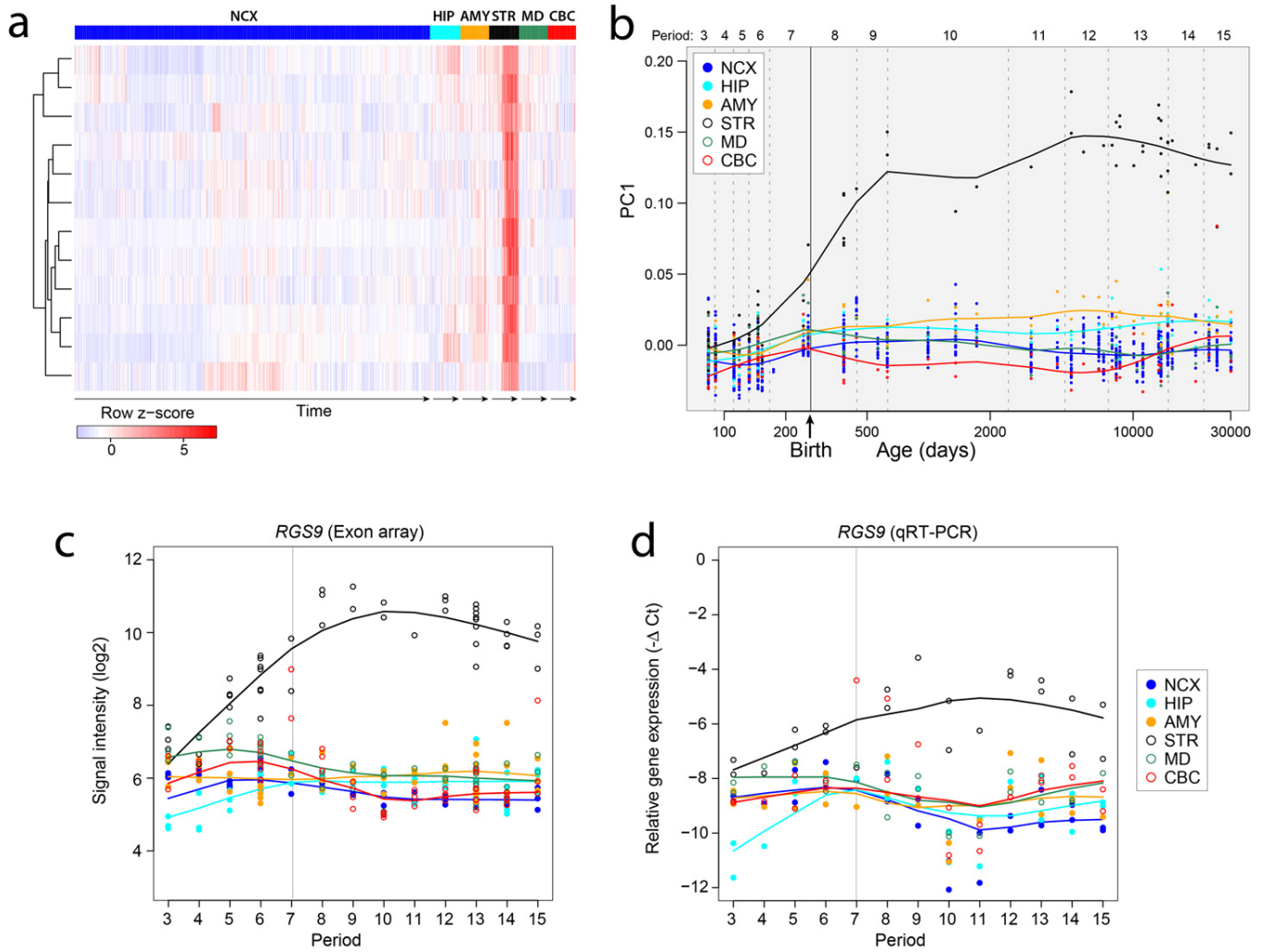
Supplementary Figure 17 | Expression of Y and X chromosome homologues in male and female brain. Ratio of male vs female median expression of protein-coding genes in all analyzed regions and NCX of male and female brain during fetal development (periods 3-7), postnatal development (periods 8-12), and adulthood (periods 13-15). One circle represents one protein-coding gene surveyed in this study. The largest differences were attributable to Y chromosome genes *PCDH11Y*, *RPS4Y1*, *USP9Y*, *DDX3Y*, *NLGN4Y*, *UTY*, *EIF1AY*, and *ZFY* (blue circles), which displayed a robust and constant expression differences across development and adulthood. Interestingly, with the exception of zinc finger X-chromosomal protein (*ZFX*), we observed that their functional homologues on the X chromosome (*PCDH11X*, *RPS4X*, *USP9X*, *DDX3X*, *NLGN4X*, *UTX*, and *EIF1AX*) were expressed at comparable levels in male and female brains across different regions and periods (Supplementary Table 7), indicating that in general these X chromosome homologues are not upregulated in a compensatory manner in developing or adult female brains.
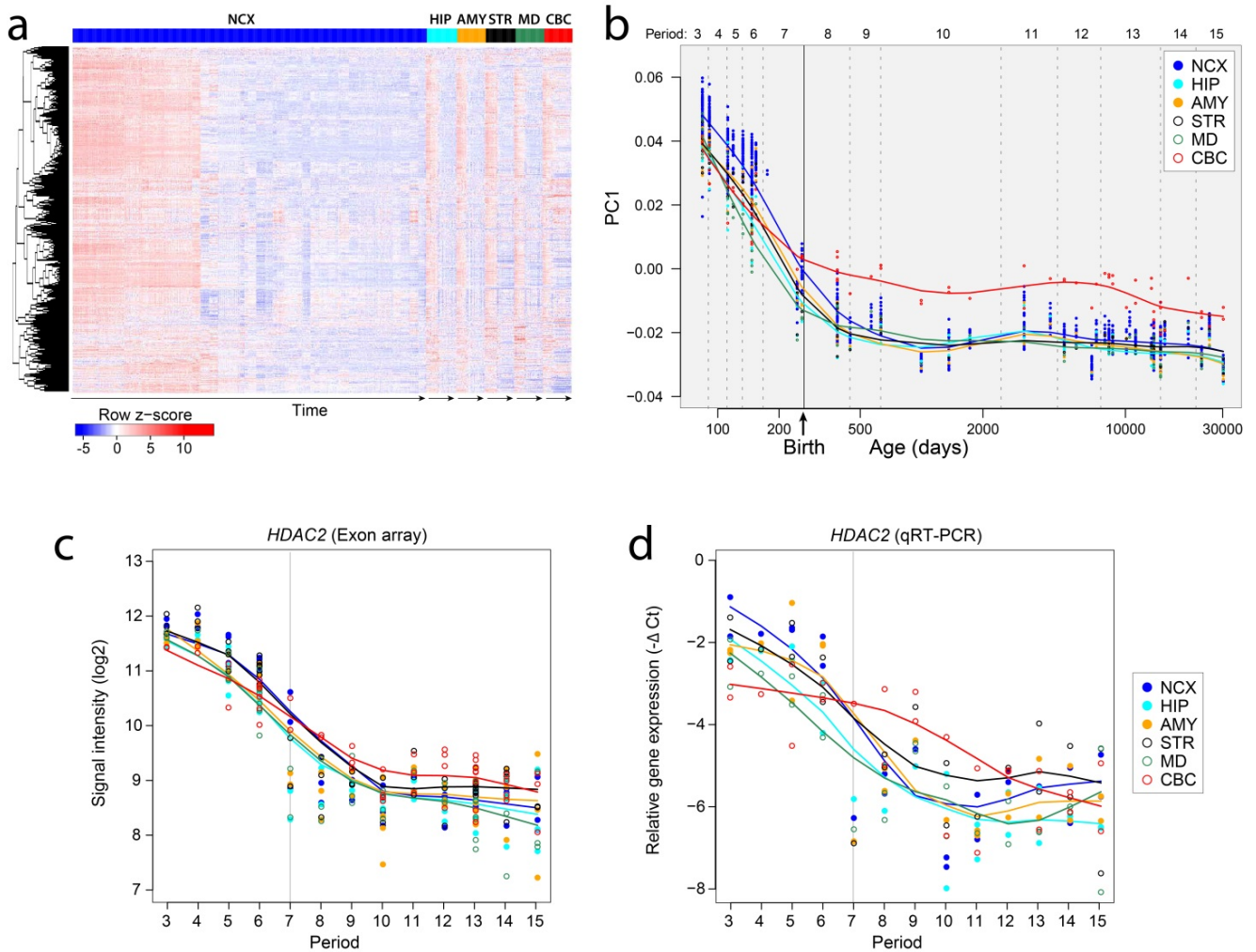
Supplementary Figure 18 | WGCNA Module 9. M9 was associated with a specific enrichment in the MD. **a,** Heat map of genes in M9 after hierarchical clustering showing the spatio-temporal pattern of the module. The expression values for each gene were ordered first by brain regions, then by age, and last by NCX areas. **b,** The spatio-temporal pattern of M9 was summarized using PCA analysis. The first principal component (PC1) was plotted against age, after being grouped and color-coded according to brain regions. The pattern was summarized by the smoothed curves of PC1 values. Dashed lines represent division between periods of the development, and the solid line separates prenatal from postnatal periods. **c, d,** Analysis of spatio-temporal expression of a representative gene, *RGS16*, with high intramodular connectivity revealed a similar pattern to the one observed for the entire module. Line plots show the log$_2$-transformed exon array signal intensity (c) and relative expression level of quantitative RT-PCR (-ΔCt) during periods 3-15 (d).
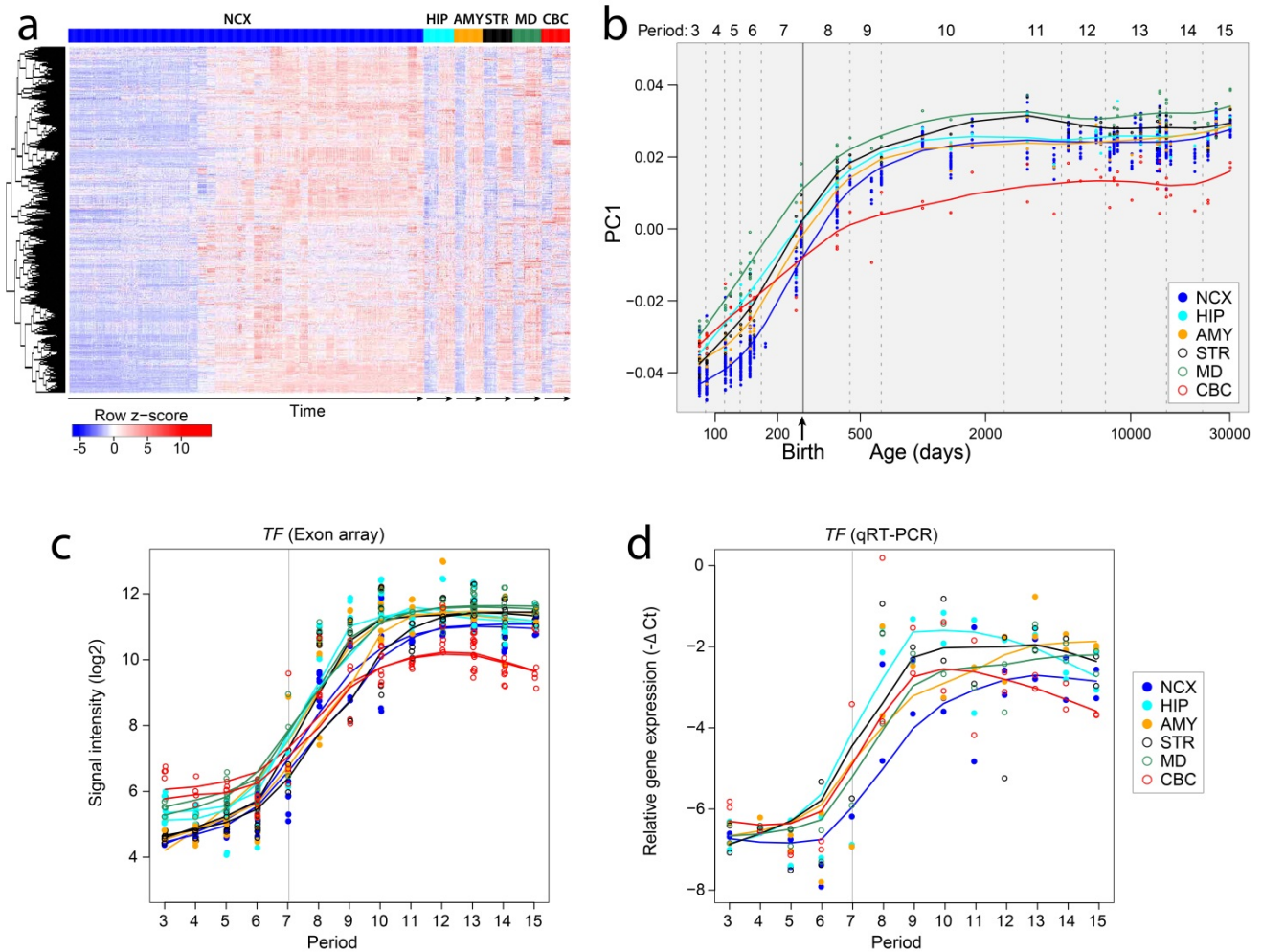
Supplementary Figure 19 | WGCNA Module 19. M19 was associated with a specific enrichment in the CBC. **a,** Heat map of genes in M19 after hierarchical clustering showing the spatio-temporal pattern of the module. The expression values for each gene were ordered first by brain regions, then by age, and last by NCX areas. **b**, The spatio-temporal pattern of M19 was summarized using PCA analysis. The first principal component (PC1) was plotted against age, after being grouped and color-coded according to brain regions. The pattern was summarized by the smoothed curves of PC1 values. Dashed lines represent division between periods of the development, and the solid line separates prenatal from postnatal periods. **c**, **d,** Analysis of spatio-temporal expression of a representative gene, *GABRA6*, with high intramodular connectivity revealed a similar pattern to the one observed for the entire module. Line plots show the log₂-transformed exon array signal intensity (c) and relative expression level of quantitative RT-PCR (-ΔCt) during periods 3-15 (d).
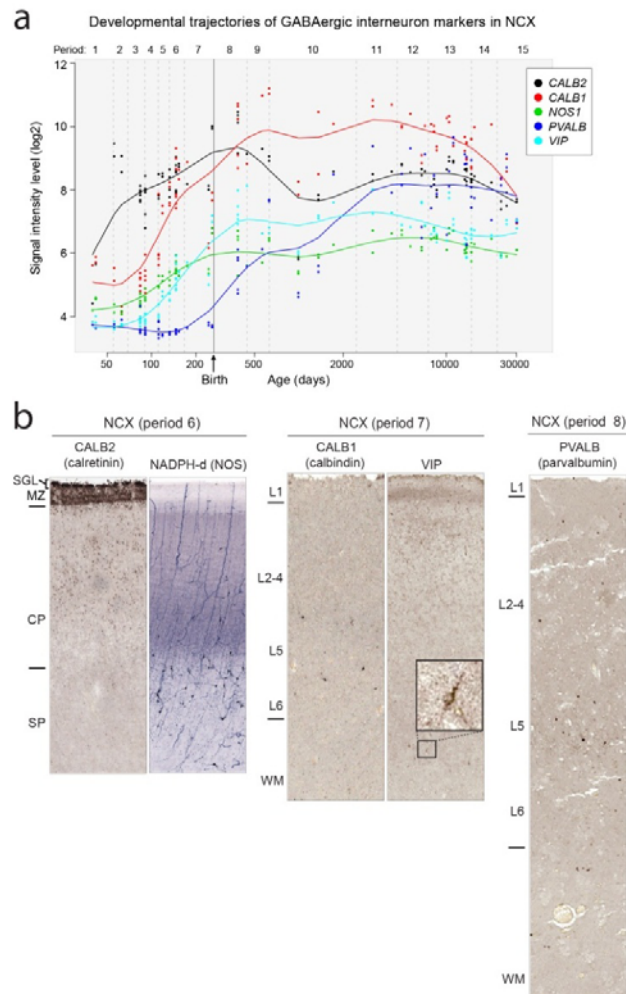
Supplementary Figure 20 | WGCNA Module 23. M23 was associated with a specific enrichment in the STR. **a,** Heat map of genes in M23 after hierarchical clustering showing the spatio-temporal pattern of the module. The expression values for each gene were ordered first by brain regions, then by age, and last by NCX areas. **b,** The spatio-temporal pattern of M23 was summarized using PCA analysis. The first principal component (PC1) was plotted against age, after being grouped and color-coded according to brain regions. The pattern was summarized by the smoothed curves of PC1 values. Dashed lines represent division between periods of the development, and the solid line separates prenatal from postnatal periods. **c**, **d,** Analysis of spatio-temporal expression of a representative gene, *RGS9*, with high intramodular connectivity revealed a similar pattern to the one observed for the entire module. Line plots show the log2-transformed exon array signal intensity (c) and relative expression level of quantitative RT-PCR (-ΔCt) during periods 3-15 (d).
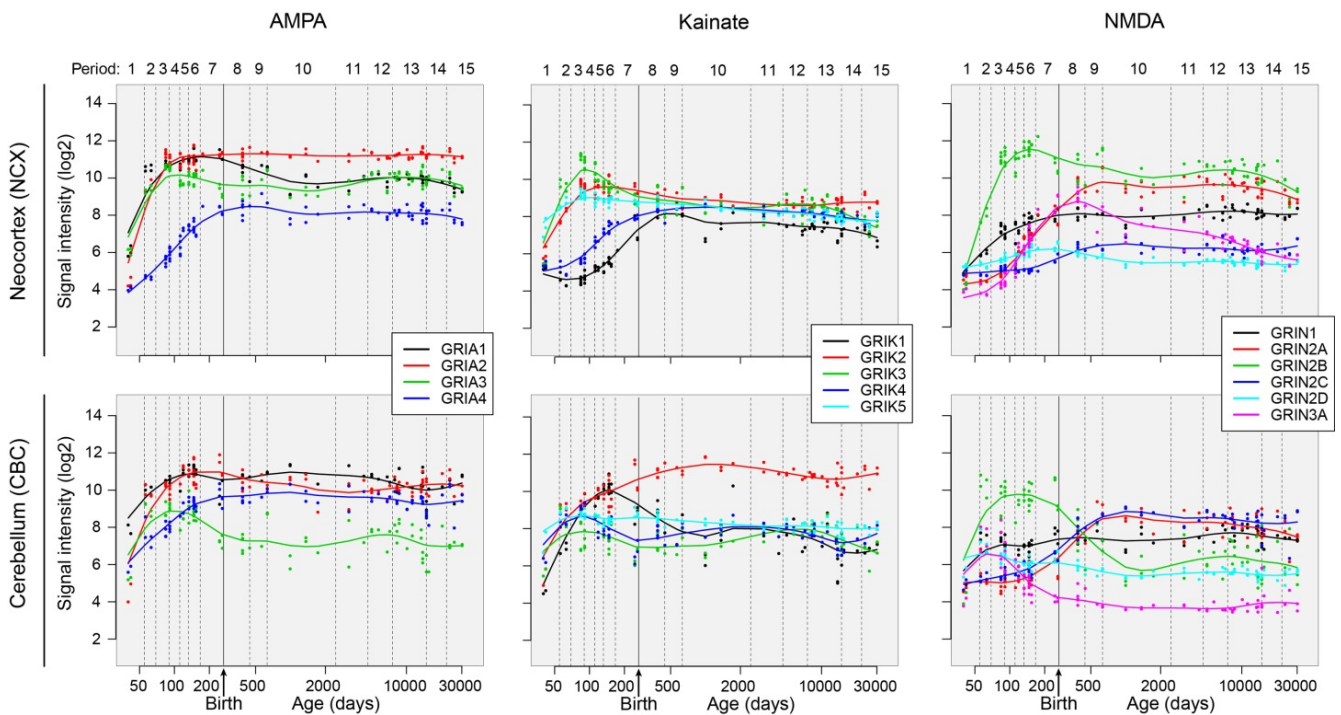
Supplementary Figure 21 | WGCNA Module 20. M20 was associated with a progressive decrease in gene expression across all regions starting from the embryonic period. **a,** Heat map of genes in M20 after hierarchical clustering showing the temporally co-expressed pattern is consistent across all regions. The expression values for each gene were ordered first by brain regions, then by age, and last by NCX areas. **b,** The spatio-temporal pattern of M20 was summarized using PCA analysis. The first principal component (PC1) was plotted against age, after being grouped and color-coded according to brain regions. The pattern was summarized by the smoothed curves of PC1 values. Dashed lines represent division between periods of the development, and the solid line separates prenatal from postnatal periods. **c, d,** Analysis of spatio-temporal expression of a representative gene, *HDAC2*, with high intramodular connectivity revealed a similar pattern to the one observed for the entire module. Line plots show the $\log_2$-transformed exon array signal intensity (c) and relative expression level of quantitative RT-PCR ($-\Delta$Ct) during periods 3-15 (d).

Supplementary Figure 22 | WGCNA Module 2. M2 was associated with a progressive increase in gene expression across all regions starting at the embryonic period. **a,** Heat map of genes in M2 after hierarchical clustering showing the temporally co-expressed pattern is consistent across all regions. The expression values for each gene were ordered first by brain regions, then by age, and last by NCX areas. **b,** The spatio-temporal pattern of M2 was summarized using PCA analysis. PC1 was plotted against age, after being grouped and color-coded according to brain regions. The pattern was summarized by the smoothed curves of PC1 values. Dashed lines represent division between periods of the development, and the solid line separates prenatal from postnatal periods. **c, d,** Analysis of spatio-temporal expression of a representative gene, *TF*, with high intramodular connectivity revealed a similar pattern to the one observed for the entire module. Line plots show the log$_2$-transformed exon array signal intensity (c) and relative expression level of quantitative RT-PCR (-ΔCt) during periods 3-15 (d).

Supplementary Figure 23 | Expression trajectories of genes associated with specific cortical GABAergic interneuron subclasses. a, Transcriptome-based expression trajectories for commonly used markers of different subclasses of cortical GABAergic inhibitory neurons. **b,** Representative images of immunohistochemical detection of CALB2 (calretinin; Swant 6B3; 1:2000), NADPH-d (a histochemical marker of NOS, including NOS1), CALB1 (calbindin; Swant 300, 1:1000), VIP (vasoactive intestinal peptide; Abcam ab8795, 1:20), and PVALB (parvalbumin; Swant PV235, 1:5000) in the NCX during periods 6-8. Expression trajectories were reminiscent of the changes in the immunohistochemical detection of interneuronal markers in the fetal and early postnatal human NCX. Of the cortical GABAergic interneuron markers analyzed in this study, *CALB2* gene expression was higher than the other markers during periods 1 and 2 (black line in a). Consistently, CALB2-immunopositive interneurons were the most abundant of the analyzed marker of GABAergic interneuron cell types in the NCX during midfetal periods (**b**). Notably, CALB2-immunopositive cells were numerous in the upper part of the cortical plate (CP). Conversely, NADPH-d/NOS1-positive interneurons were less abundant than CALB2-immunopositive interneurons (green line in a). Although some NOS1-positive cells were found in deeper layers of the CP, the majority was found in the CP-subplate (SP) border. Consistent with the gene expression data and previous independent immunohistochemical studies[73], CALB1- and VIP-immunopositive interneurons were the next to be detected in the NCX and can be easily identified during period 7. *PVALB* expression (dark blue line in a) and immunohistochemical staining (b) were the last to be detected in the NCX around birth. (SGL; subpial granular layer, MZ; marginal zone, L; layer, WM; white matter)

Supplementary Figure 24 | Expression trajectories of genes encoding the subunits of glutamate receptors. Expression levels of different subunits of ionotropic glutamatergic receptors (AMPA, Kainate and NMDA) are shown for neocortex and cerebellum. Most subunits started to be expressed early during development and remained expressed throughout entire lifespan. However, spatio-temporal differences in expression patterns of different subunits were observed. Note that *GRIN3A* in CBC was the only subunit that appeared not to be expressed in postnatal or adult period.
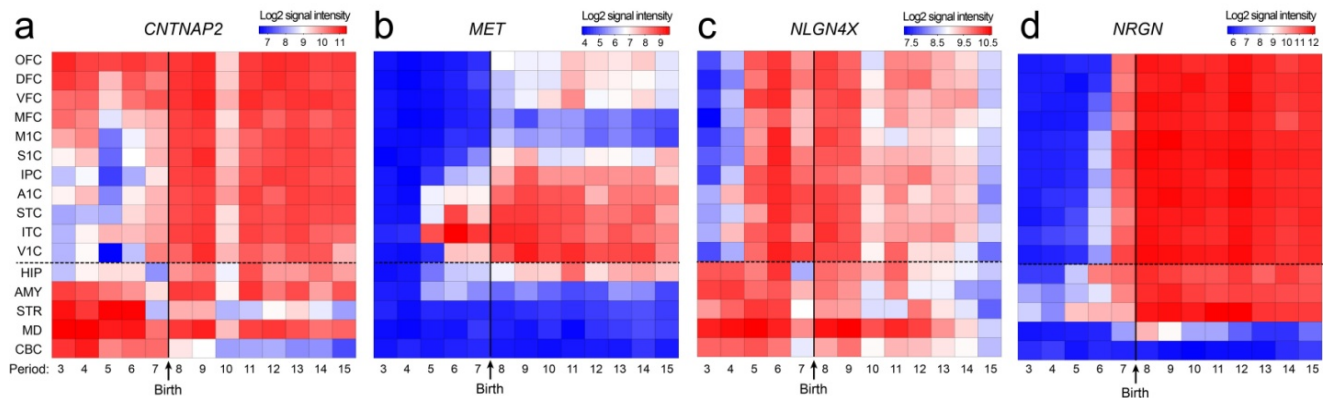
Figure 25 | Spatio-temporal expression patterns of disease-related genes. a-d, Heat map matrix representations of spatio-temporal expression of representative genes whose variants have been previously linked to (a-c) ASD (*CNTNAP2, MET, NLGN4AX*) and (d) schizophrenia (*NRGN*). The expression images display log$_2$-transformed signal intensity across analyzed regions/areas and time periods using a heat map color scale from low (blue) to high (red). The dashed horizontal line separates NCX areas from other brain regions. The birth time is marked by vertical solid line. **a**, *CNTNAP2*, which encodes a neurexin family protein implicated in ASD, was highly enriched in the areas of the fetal OFC and DFC, as previously reported[15,17]. The expression levels of *CNTNAP2* suddenly increased in other cortical areas during early infancy (period 8), after which it remained expressed in all NCX areas. **b**, *MET*, which encodes a hepatocyte growth factor receptor, has been linked to ASD[74] and exhibited a partially overlapping but distinct NCX areal expression pattern. *MET* was highly enriched in the early midfetal ITC and then increased in the surrounding temporal-occipital areas and the OFC, where it remained enriched throughout development. **c**, *NLGN4X*, a gene encoding a protein involved in synapse formation and function[75], was upregulated during the second half of the prenatal NCX development, which coincided with an increase in the expression of genes associated with synapse and dendrite development (Fig. 5 b, c). *NLGN4X* was also identified as a sex-specific DEU gene (Fig. 3). Mutations in *NLGN4X* have previously been associated with ASD, which are more prevalent in males. Many of the ASD-associated risk SNPs and deletions were present in exons 5, 6, and 7 *NLGN4X*[76,77], which displayed male-biased DEU. **d**, *NRGN*[40], which encodes a postsynaptic protein kinase substrate, was highly expressed in all NCX areas starting after birth, progressively increased in expression until late childhood, and remained well-expressed in adulthood.